
Masters Theses


Student Theses and Dissertations

Summer 2016

Synthesis and photonic sintering of bioresorbable zinc nanoparticle ink for transient electronics manufacturing

Bikram K. Mahajan

Follow this and additional works at: https://scholarsmine.mst.edu/masters_theses

 Part of the [Materials Science and Engineering Commons](#), [Mechanical Engineering Commons](#), and the [Nanoscience and Nanotechnology Commons](#)

Department:

Recommended Citation

Mahajan, Bikram K., "Synthesis and photonic sintering of bioresorbable zinc nanoparticle ink for transient electronics manufacturing" (2016). *Masters Theses*. 7857.
https://scholarsmine.mst.edu/masters_theses/7857

This thesis is brought to you by Scholars' Mine, a service of the Missouri S&T Library and Learning Resources. This work is protected by U. S. Copyright Law. Unauthorized use including reproduction for redistribution requires the permission of the copyright holder. For more information, please contact scholarsmine@mst.edu.

SYNTHESIS AND PHOTONIC SINTERING OF BIORESORBABLE ZINC
NANOPARTICLE INK FOR TRANSIENT ELECTRONICS MANUFACTURING

by

BIKRAM KISHORE MAHAJAN

A THESIS

Presented to the Faculty of the Graduate School of the
MISSOURI UNIVERSITY OF SCIENCE AND TECHNOLOGY

In Partial Fulfillment of the Requirements for the Degree

MASTER OF SCIENCE IN MECHANICAL ENGINEERING

2016

Approved by

Heng Pan, Advisor
Xian Huang, Co-Advisor
Hai-Lung Tsai
Fuewen Frank Liou

© 2016

Bikram Kishore Mahajan

All Rights Reserved

PUBLICATION THESIS OPTION

This thesis has been prepared in the form of two papers using the styles utilized by the following publications:

Paper I, Pages 9-28 are intended for submission in ACS NANO

Paper II, Pages 29-50 are intended for submission in ADVANCED MATERIALS

ABSTRACT

Zinc is an essential ‘trace element’ that supports immune systems, and is required for DNA synthesis, cell division, and protein synthesis. Zinc nanoparticles (Zn NP) has antibacterial properties and potential to be used in biodegradable printed electronics devices. The research presented here is about the synthesis of Zn NP and their potential use in transient electronics devices. In Paper 1, a technique of room temperature synthesis of Zn NP is reported using ball milling. Controlled amount of PVP was mixed in the solvent to stabilize the Zn particles and minimize cold welding during milling. The size of the produced Zn NPs was found to be heavily dependent on the amount of PVP used in the solvent. The analyses reveals a crystal size of $\sim 34.834 \pm 1.76$ nm and very low oxidation in the Zn NPs. The obtained Zn NPs were directly used to print bioresorbable patterns on Na-CMC and PVA substrates which forms conductive patterns upon subjecting to photonic sintering. In paper 2, a new method of manufacturing transient electronics devices is reported. An aerosol printer has been used to print patterns using Zn NPs based bioresorbable ink. Lower concentration of PVP used results in the formation of surface oxide, while higher concentration of PVP hinders the coalescence of Zn NPs. Conductivity of about 0.1% to that of bulk has been found when 0.1 wt % PVP is used. Analytical simulations has been accompanied with experimental verifications in the study of sintering mechanism of Zn NPs. XPS analysis indicates Zn NP surface protection by PVP. The ink was used to print patterns which can potentially be used as RFID tags, on a biodegradable Na-CMC substrate. The whole substrate dissolves in water.

ACKNOWLEDGMENTS

I would like to express my deepest gratitude to my advisor, Dr. Heng Pan, for giving me an opportunity to do research in his laboratory. His constant inspiration, diligent mentoring and support has encouraged me throughout the course of this research work. I would also like to thank my co-advisor Dr. Xian Huang for introducing me to the very exciting field of transient and flexible electronics. I really appreciate all the hard work that my advisor and my co-advisor has done, even outside the usual office hours, to make me understand the intricacies of the projects.

I wish to thank Dr. Hai-Lung Tsai and Dr. Fuewen Frank Liou for serving in my committee and taking their time to read my thesis and providing valuable insights which were very helpful.

I wish to thank my lab mates Brandon Ludwig, Xiaowei Yu, and Wan Shou for continuous support, technical discussions and help with writing the thesis and understanding the topics. I would also like to thank all my friends who have patiently extended all sorts of help for accomplishing this undertaking.

I would like to thank my family for all the love and encouragement. They have always supported me and I admire their sacrifice. I am really grateful to my cousin, sister-in-law and Susmita for all their help and support, from the day 1 of my graduate school.

TABLE OF CONTENTS

	Page
PUBLICATION THESIS OPTION.....	iii
ABSTRACT.....	iv
ACKNOWLEDGMENTS	v
LIST OF ILLUSTRATIONS.....	viii
 SECTION	
1. INTRODUCTION	1
1.1. ZINC	1
1.2. BALL MILLING TECHNIQUE	2
1.3. AEROSOL PRINTING	4
1.4. PHOTONIC SINTERING	5
2. SCOPE AND OBJECTIVE:.....	7
 PAPER	
I. ROOM TEMPERATURE SYNTHESIS OF NANOCRYSTALLINE ZINC BY WET MILLING FOR PRINTED BIORESORBABLE ELECTRONICS AND BIOMEDICAL APPLICATIONS	9
ABSTRACT.....	9
INTRODUCTION	10
RESULTS AND DISCUSSION.....	12
CONCLUSION.....	23
MATERIALS AND METHODS.....	24
Ball Milling Of Zinc	24

Water Soluble Substrate Preparation	24
Structure Characterizations	25
Diffraction And Spectroscopy	25
Thermal Analysis	25
Photonic Sintering.....	25
ACKNOWLEDGEMENT	25
REFERENCES	26
II. Photonic Sintering Of Bioresorbable Zinc Nanoparticle Ink For Transient Electronics	
Manufacturing.....	29
ABSTRACT.....	29
EXPERIMENTAL SECTION	33
DISCUSSION.....	34
CONCLUSION.....	47
ACKNOWLEDGEMENT	48
REFERENCES	48
SECTION	
3. CONCLUSION.....	51
REFERENCES	52
VITA.....	58

LIST OF ILLUSTRATIONS

Figure	Page
PAPER I	
1. (a) Flow chart of the experiments. Morphology of zinc particles milled for (b) 0 hours (c) 9 hours (d) 18 hours (e) 27 hours and (f) 36 hours. (g) Average particle diameter (as calculated by ImageJ) as a function of milling time.	13
2. Physical and chemical characterizations of ball milled zinc samples. The scale is of 2 μ m for figure (a) and (b). SEM image of the ball milled sample with (a) No PVP (b) 1 wt % PVP in the solution. (c) XRD spectra of the as received Zn microparticles, samples ball milled for 36 hours with no PVP and 0.1 wt% PVP (d) TG-DTA characterizations of the Zn produced by 36 hours of milling (e) TEM image of the samples ball milled for 36 hours and SAED pattern of the selected area (in inset) (f) HRTEM image of the samples showing crystallite structures with dashed lines.....	16
3. (a) XPS survey spectrum of the sample ball milled for 36 hours. High resolution XPS spectra of (b) carbon (c) oxygen (d) zinc.	19
4. Morphology and characterizations of flash sintered ball milled zinc samples. The scale is of 2 μ m for all images. The scale is 0.5mm for the images in the inset (a) as deposited samples. Samples flash sintered once at a voltage of (b) 1.8kV (10.18 J/cm ²) (c) 2kV (14.15 J/cm ²) (d) 2.2 kV (18.98 J/cm ²) (e) 2.3 kV (20.7 J/cm ²) and (f) 2.5 kV (25.88 J/cm ²). (g) Average particle diameter and (h) conductivity as function of increasing energy when subjected to photonic sintering in argon environment.	20
5. (a) Stable ball milled ink in a glass bottle before printing (b) Pattern printed on a flexible and bendable substrate (c) The pattern dissolving in water in about 3 hours. (d) Pattern dissolving in water in about 12 hours when mounted on Na-CMC substrate..	22
PAPER II	
1. Overview of the new process for transient electronics manufacturing. (a) The set-up for aerosol printing and photonic sintering (b) As deposited Zn nanoparticles with 0.1 wt% PVP (c) Sintered Zn nanoparticles with 1 Flash at 20.7 J/cm ² . The scale is of 4 μ m (d) Resistance study of the sample (e) Transient behavior of the sample.	36

2. PVP effects on flash annealed structures (in Argon). The mechanism: PVP helps reduce surface zinc oxide to allow coalescence; too much PVP will form matrix that prevents zinc coalescence; too less PVP (high surface oxide) will prevents zinc coalescence. The scale is $5\mu\text{m}$. Aerosol printed patterns with (a) 0 wt % PVP (b) 0.1 wt % PVP (c) 1 wt% PVP. They were flashed once at 10.18, 17.89 and 20.7 J/cm^2 . The last picture represents the model of the Zn NPS after flashing once at 20.7 J/cm^2 (d) the average particle diameter with increasing flash voltage. (e) Resistance study of the samples with different PVP concentration..... 37
3. Composition analysis of the annealed Zn in Argon and Ambient. The scale is $2\mu\text{m}$ for the cross-section view of the as-printed aerosol patterns. High resolution XPS spectra of C, N, O and Zn of Zn NPs annealed in argon environment 39
4. Composition analysis of the annealed Zn in Ambient. (a) Top View of Zn NPs annealed in ambient. (b) Resistivity study of 0 wt% PVP, 0.1 wt% PVP and 1 wt% PVP annealed in ambient. ((c) High resolution XPS spectra for C1s, O1s and Zn2p for annealed samples..... 42
5. Melting and sintering mechanism and melt depth (simulation and experiments). (a) Generated model comprising of Zn NPs on a $10\mu\text{m}$ glass substrate in Argon environment before heating. Simulation of sintering mechanism (b) thin layer (c) thick layer of Zn NPs in Argon environment at different time interval. (d) Temperature profile for thick and thin layer of Zn NPs generated from simulation. SEM Image of (e) a thin layer and a (f) thick layer of Zn NPs on glass, flashing at 20.7 J/cm^2 44
6. Adhesion study of Zn with Na-CMC and transient behavior. Zn NPs gets into Na-CMC with increasing Flash voltage. (a) as deposited sample (b) 1 Flash at 18.98 J/cm^2 (c) 1 Flash at 20.7 J/cm^2 . (d) An EDS image is shown at inset where Zn nanostructures getting embedded in the substrate CMC (e) The substrate fully disappears in about 12 hours. 46

1. INTRODUCTION

1.1 ZINC

Zinc Oxide (ZnO) is a wide band-gap oxide semiconductor (3.37 eV) [1] with a high excitation binding energy (60 meV) [2] and has numerous applications in non-volatile memory[3], solar cells[4], light emitting diodes[5], photodetectors[6], gas sensors[7], photocatalytic activities[8], cosmetics [9] etc. The ease of controlling the growth of ZnO nanostructures such as nanoparticles, nanowires, nanotubes, nanorods etc. is the reason why ZnO has been in focus for research activities in last few decades. However, less attention is paid to the synthesis of Zinc nanostructures compared to ZnO nanostructures, even though Zn is credited as one of the ‘most essential trace elements’ for the vital functions in the physiological activities in human. Zinc nanoparticles (Zn NPs) has broad and diverse applications in molecular diagnostics [10], drug delivery [11], [12], and developing new drug [13]. It has also been demonstrated theoretically that Zn NPs possess high stability and quantum size effects [14]. Besides that, Zn NPs also exhibit outstanding antibacterial efficacy[15], anticorrosion properties [16], and have been used as a catalyst for the decomposition of ammonium perchlorate in a propellant [17]. Zn NP has potential to be used in batteries for medical devices [22], printed circuit boards [23] and implantable devices such as stents [24]. Moreover Zn NPs belongs to the special section of materials which are biodegradable [18], [19] and has promising future in the developing bio-resorbable electronics devices (transient electronics devices), [20] [21] which operate over a short period of time (tunable from minutes to weeks) and dissolve afterward into biologically safe compounds. As of now, the transient electronics devices are predominantly fabricated by complex, time-consuming process based on anhydrous

surface micromachining and complementary metal–oxide–semiconductor (CMOS) fabrication techniques on regular substrates (Silicon) followed by transfer printing to bio-resorbable substrates. Zn NPs can be used to make bio resorbable inks which can be printed directly on bio-resorbable substrates thus paving the way for mass manufacturing, high-quality and low cost transient electronics devices. Also fully resorbable electronic devices and multilayer bio-resorbable printed circuits boards based on Zn and other metals has recently been demonstrated[22]. Thus in addition to various other applications, Zn NPs is also very important for developing innovative healthcare products and environment friendly electronics devices.

Approaches in synthesizing Zn NPs and controlling their sizes and morphology include metal-ligand-coordinated vesicle phase[23], UV laser irradiation of ZnO [24], laser ablation [25][26], plasma in liquid [27], organometallic precursor[28], bio-reduction [29], lithium reduction [17] laser assisted chemical vapor deposition[30], and electrodeposition[31] etc. Although high purity and highly crystalline structure have been produced by some of these methods, they require high vacuum of 1×10^{-7} Torr [30] or high pressure of 20KPa [27] or handling potentially hazardous chemicals such as Zinc Laurate [23], Hydrochloric acid [29], Lithium Borohydride [32] etc. or expensive experimental set up such as laser[24], [30], electrodeposition [31] etc. Hence synthesizing Zn NPs using a simple, inexpensive, room-temperature and large-scale process which does not require handling dangerous chemicals, is very important.

1.2. BALL MILLING TECHNIQUE

A preferred technique for nano-crystalline material synthesis involves planetary ball milling, which is a high energy milling process featuring high yield, low cost, and room temperature operation. Planetary ball milling uses a circular platform rotating in

one direction and vials with grinding media and powders rotating in reverse direction. The resulting centrifugal force causes impact and friction of milling balls, leading to fractures of milled powders through high energy collision as well as reduction in particle sizes from micro to nanoscales. Ball milling process is subjected to influence of several critical parameters such as milling duration, milling interval, ball-to-powder ratio, rotation speed, milling ball size, and milling atmosphere, all of which are combined to determine quality, yield, and reproducibility of the resulting nanoparticles. Ball milling technique has been successfully implemented to fabricate ZnO nanoparticles [33]–[37]. However, fabricating Zn NPs through ball milling technique has not yet been thoroughly studied. Challenges involved in the ball milling process of zinc include particle agglomeration [ref] and cold-welding [38]. The former is caused by increased electrostatic effect and interactions between molecules with reduced particle sizes, while the latter is due to atom diffusion between interfaces of particles, especially when zinc undergoes transition from a brittle material to ductile material at certain temperature range (~100-150°C). To overcome above mentioned challenges, process control agents (PCA) and proper temperature control should be introduced during the milling process. Dry milling of zinc is infeasible as lack of media to dispersing PCA and intense cold welding phenomena. Zn NPs has been generated through cryomilling [39]–[43] and combination of cryomilling and room temperature milling [38]. However, cryomilling requires specially designed vial with liquid nitrogen jackets or pipelines running along the vial or the mill, making the process complicated and increasing the cost of production. Also the powder quality produced by cryomilling was inhomogeneous and the yield was low. Additionally, dead zones were formed in the tank and excessive powder loss occurred due to liquid nitrogen evaporation

and flow control. Also freezing of the apparatus and jamming occurs quite often, which makes the process unreliable for large scale production [44].

1.3. AEROSOL PRINTING

Direct writing or maskless printing, a technique widely used in printed electronics, deposit functional materials to form scalable patterns on a substrate. They offer more flexibility, scalability, speed and are relatively cheaper than the traditional lithography-based technologies. Although Inkjet printing is the most mature form of direct writing, the newly developed aerosol jet printing (AJP) comes with its own advantages like highly focused and continuous stream of ink, minimal nozzle clogging due to the use of sheath gas, wider viscosity range of the compatible ink (0.5 to 2500 cP)[45], compatibility of three-dimensional nonplanar substrates in the millimeter range, etc. Moreover, the non-contact deposition technique of AJP is completely scalable technique and yields high throughput. It has already been used in flexible displays, thin-film transistors, circuits, multilayer ceramic capacitors (MLCCs)[46] and biological sensors[47]. In AJP, the nanoparticle is placed into a pneumatic nebulizer, which creates dense (10^7 drop/cm³) aerosol droplets ranging from few hundred nanometers to micrometers. The smaller aerosol droplets are carried to the nozzle head by the carrier N₂ gas flow, while the rest of the droplets drop back to the ink and are recycled. The aerosol is aerodynamically focused in the nozzle head, which creates an annular flow of N₂ to collimate the aerosol beam ensuring a continuous stream out of the nozzle. The distance between the nozzle head and the substrate can be varied upon requirements. The substrate, mounted on a stage controller, which can be programmed directly from CAD models to move in different directions at different speeds (ranging from 0.01 mm/sec to 25mm/sec) to form the desired patterns on bioresorbable films.

1.4. PHOTONIC SINTERING

The printed bioresorbable inks can be sintered by photonics sintering⁴⁶ methods, which offer various unique advantages over other existing methods, such as furnace heating[48], selective laser[49], direct-current[50], and microwave[51]. For example, the furnace sintering is slow, and involves high temperatures that will cause damage and deformation of the bioresorbable substrates, which have low melting temperatures (<100°C). Selective laser sintering constrains the heating locally by focusing the laser beam strictly to the printed traces, but it is technically complex and inefficient both in time and cost. In addition, the high energy intensity may also cause the potential damage to the bioresorbable substrates that are directly underneath the sintering patterns. Direct current sintering and microwave sintering use either the resistive heating or interaction between nanoparticles with electromagnetic field. However, both methods require initial conductivity in the sintered materials and suffer from inhomogeneities that may lead to local overheating and damage to the structures. Photonic sintering exploits the distinctly different light absorption properties of the inks and the substrates in a wide spectrum region. Whereas bioresorbable substrates are typically transparent, nanoparticle inks are deeply colored and strongly absorb visible light. Using xenon lamp, instant high temperatures can be achieved in the ink patterns over large exposed areas within a few hundred microseconds or a few milliseconds, resulting in a substantial sintering process with only very limited influence to the properties of the substrates. Photonic sintering has been used to anneal conductive nanoparticles, such as gold [52], silver[53] and copper[54], as well as dielectric nanoparticles (e.g. alumina, zirconia, barium titanate, and mica). Photonic sintering is built on three assumptions about nanoparticles under sintering. First, the bioresorbable nanoparticles are predominantly black, thus most photonic energy has

been absorbed rather than scattered. In addition, due to the high surface area to mass ratio, the nanoparticles will be heated easily and sintered quickly. Furthermore, as the nanoparticle films are very thin, they have limited heat retention capability and cool rapidly, minimizing damage to the underneath substrates. The photonic sintering of nanoparticles is a combined effect from the melting point depression and absorption characteristics of the nanoparticles. Melting point depression is a feature of metal nanoparticles where the melting points of the particles depend on the sizes of the particle and are lower than that of the bulk metal, while the absorption characteristics refers to wavelength-dependent photonic energy absorption by the nanoparticles, which causes significantly periodical displacement of electrons and subsequent heat generation. Although photonic sintering has not yet been used for sintering bioresorbable inks, several features of the bioresorbable inks including melting point depression and strong photonic absorption suggest great potential in sintering bioresorbable inks through the photonics method.

2. SCOPE AND OBJECTIVE

In the first part, a room temperature synthesis approach of Zn NPs through ball milling using Polyvinyl-pyrrolidone (PVP) as a process control agent (PCA) in a wet milling condition is reported. PVP can wrap around particles and inhibits the cold wetting of nanoparticles [55]–[60], while a wet milling condition offers mutual repulsed polar ions around the nanoparticles to prevent agglomeration of Zn NPs. However, both the amount of PVP and the milling process have to be well characterized in order to achieve optimized conditions to yield stable and repeatable results of controlled particle sizes. The PVP also doubles as a binder for the bio-resorbable Zn NPs based ink which can be used for direct printing on bio-degradable substrates for electronics devices. Although bulk zinc has a melting point of 419.53 °C, Zn NPs will have melting point depression based on their size. The NPs can be photonic sintered to form conductive patterns, without degrading the substrate itself and can be potentially used for mass-manufacturing various bio-degradable electronic devices. The optimum amount of PVP and ball milling parameters are investigated, and the characteristics of the milled nanoparticles systematically analyzed in this report. The Zn NPs were then printed on bio-degradable substrate (sodium carboxymethyl cellulose or Na-CMC) to figure demonstrate a simple resistance. The studies have shown remarkable results which might have significant impact to the preparation of Zn NPs with a high yield and photonic sintering to obtain various electronic devices for use in various applications.

In the second part, a new method of manufacturing transient electronics devices is reported. An aerosol printer has been used to print patterns using Zn NPs based bioresorbable ink. The amount of stabilizer and capping agent (PVP) used in the synthesis

of the ink was found to be of vital importance during sintering. Lower concentration of PVP results in the formation of surface oxide, while higher concentration of PVP hinders the coalescence of Zn NPs. Different PVP concentrations (0, 0.1 and 1 wt% of the entire ink) has been investigated. Resistivity of about $3.3 \times 10^{-3} \Omega\text{-cm}$ which is about 0.1% to that of bulk has been found when 0.1 wt % PVP is used. Analytical simulations has been accompanied with experimental verifications in the study of sintering mechanism of Zn NPs. Extensive XPS tudies were done to analyse the composition of different concentration of PVP as well as sintering in different environments. The interface of the conductive pattern and the substrate was studied by EDX. The ink was used to print patterns which can potentially be used as RFID tags and different kinds of resistors, on a biodegradable Na-CMC substrate. The whole substrates dissolves completely in few hours, without leaving any biologically harmful components.

PAPER

I. ROOM TEMPERATURE SYNTHESIS OF NANOCRYSTALLINE ZINC BY WET MILLING PRINTED BIORESORBABLE ELECTRONICS AND BIOMEDICAL APPLICATIONS

Bikram K Mahajan,¹ Heng Pan,^{1,} and Xian Huang^{2,*}*

¹Department of Mechanical Engineering, Missouri University of Science and Technology, Rolla, Missouri 65409, USA

²Department of Biomedical Engineering, Tianjin University, Tianjin, 300072, China

*Corresponding author

ABSTRACT

Synthesis of Zinc Nanoparticles (Zn NPs) using a cheap, reliable and high yielding technique is necessary to meet its increasing demand in biological and chemical applications. Here we report the room temperature synthesis of stable Zn NPs using ball milling. Controlled amount of PVP was mixed in the solvent to stabilize the Zn particles and minimize cold welding during milling. The size of the produced Zn NPs was found to be heavily dependent on the amount of PVP used in the solvent. Systematic morphological and compositional analysis of the Zn NPs was carried out using SEM, TEM and XRD. The analyses reveals a crystal size of $\sim 34.834 \pm 1.76$ nm and very low oxidation in the Zn NPs. XPS data confirms the existence of PVP encapsulated Zn NPs. The obtained Zn NPs were directly used to print bioresorbable patterns on Na-CMC and PVA substrates which forms conductive patterns upon subjecting to photonic sintering. Highest conductivity of 72491 S/m was obtained from the sintered samples. The samples later dissolves in water into biologically safe compounds.

INTRODUCTION

Zinc is an essential trace element that supports immune systems¹, and is required for DNA synthesis, cell division, and protein synthesis². Deficiency of zinc can rapidly diminish mediated responses of antibody and cell in human, and thus can greatly alter defense systems of human bodies³. Beside of its biological effects, readily dissolution of zinc in biofluids yields its applications as bioresorbable materials in stent⁴, bone implant⁵, and artificial joint⁶, and has inspired the use of zinc in recent development of bioresorbable electronics (or transient electronics), which operates over a short period of time (from minutes to weeks) and dissolves afterward to generate biologically safe products⁷. Fully bioresorbable electronic devices have been demonstrated both as basic components⁸ and as simple, functional circuits with applications ranging from energy storage⁹, power scavenger¹⁰, implantable sensors¹¹, and communication beacon¹², showing great promise towards fully integrated multifunctional transient circuits.

Bioresorbable electronic devices have stringent requirements for environmental humidity and temperature, and are predominately achieved by complex, time-consuming fabrication processes based on anhydrous surface micromachining and CMOS techniques¹³. Alternative methods based on printable electronics techniques offer fast prototyping, high yield, and low cost, and have been demonstrated by screen-printed wireless circuits based on conductive pastes made of Zn and W micro-particles¹⁴. The pastes achieve moderate out-of-plane conductivity through room-temperature curing, while the in-plane conductivity has yet to be satisfied, urging further improvement of device performance through transient conductive inks that containing nanoparticles, which can be sintered at low temperature without damaging the heat sensitive polymer substrates. Essential step involves synthesizing Zn NPs. However, existing approaches in synthesizing

Zn NPs are either required high temperature¹⁵ or high pressure¹⁶. Expensive and complex equipment is typically demanded¹⁷⁻¹⁹, showing high cost and low effectiveness.

A preferred technique for nano-crystalline material synthesis involves high energy planetary ball milling, which uses counteracted rotation of a circular platform and vials to create impact and friction of milling balls inside the vials, leading to fracture of milled powders and reduction of particle sizes. The ball milling process is subjected to influence of several critical parameters such as milling duration, milling interval, ball-to-powder ratio, rotation speed, milling ball size, and milling atmosphere, all of which are combined to determine quality and yield of the resulting nanoparticles. Ball milling technique has been successfully implemented to fabricate various nanoparticles of metal and metal oxide such as ZnO²⁰⁻²³, Cu²⁴ and Al₂O₃²⁵. However, fabricating of Zn NPs through ball milling is rarely reported, let alone study in the context of printable transient electronics. Here, we report a synthesis approach of Zn NPs through planetary ball milling using Polyvinylpyrrolidone (PVP) as a process control agent (PCA) in a wet milling condition. The amount of PVP and the milling process have been characterized to achieve optimized process conditions to yield controllable and repeatable particle sizes. The resulting nanoparticles can be used to prepare bioresorbable inks, which can be directly printed onto bioresorbable substrates for electronics devices. A novel photonic sintering method has been used to sinter bioresorbable inks prepared with milled Zn NPs, resulting in formation of continuous and conductive matrix of Zn NPs through localized heating, while maintaining the integrity of the substrate. Characterization of the nanoparticles as well as inks show promising results, suggesting potential impact of the ball milled Zn NPs in printable bioresorbable electronics.

RESULTS AND DISCUSSION

Figure 1a shows the processes to obtain Zn NPs. The processes involve dispersion of zinc particles as purchased in a solvent solution premixed with methanol, butyl acetate, and PVP, allowing the PVP to wrap around the Zn particles. The resulting solution can be milled in a planetary ball mill for 36 hours, causing the reduction of particle sizes from microscales to nanoscales. The Zn NPs can be used to prepare bioresorbable ink, which can be printed into strips predefined with Kapton tapes, following by room temperature curing to remove the solvent and photonic sintering to turn non-conductive printed patterns into conductive structures.

Effect of particle size reduction is first studied at different milling time. Figure 1b to 1f shows significant morphology changes of the zinc particles with milling time from 0 to 36 hours. The ball milling process starts with Zn microparticles with sizes ranging from $0.5\mu\text{m}$ to $10\mu\text{m}$ (Figure 1b). The milling of zinc particles occurs in several stages with distinct sizes and morphology. The first stage happens at the first 9 hours of the milling process, in which particles slide along one another with moderate deformation and fracture, producing fine irregular particles (Figure 1c). The second stage involves formation of flattened particles and considerable reduction of particle sizes due to repetitive impact of the balls with high kinetic energy and collision with the inner walls of the vials. Nanostructures usually start forming in this stage (Figure 1d and 1e). The particles reach their size limits and steady states at the final stage, in which the energy from the ball milling is in equilibrium with the energy need to create new fractures and to stop the agglomerate of the nanoparticles. Extended milling time does not further reduce the particle size, but introduce contamination from inner wall of the vials, and hence should be avoided. Figure 1g shows the average particle size distribution plotted against milling hours from 0 to 36

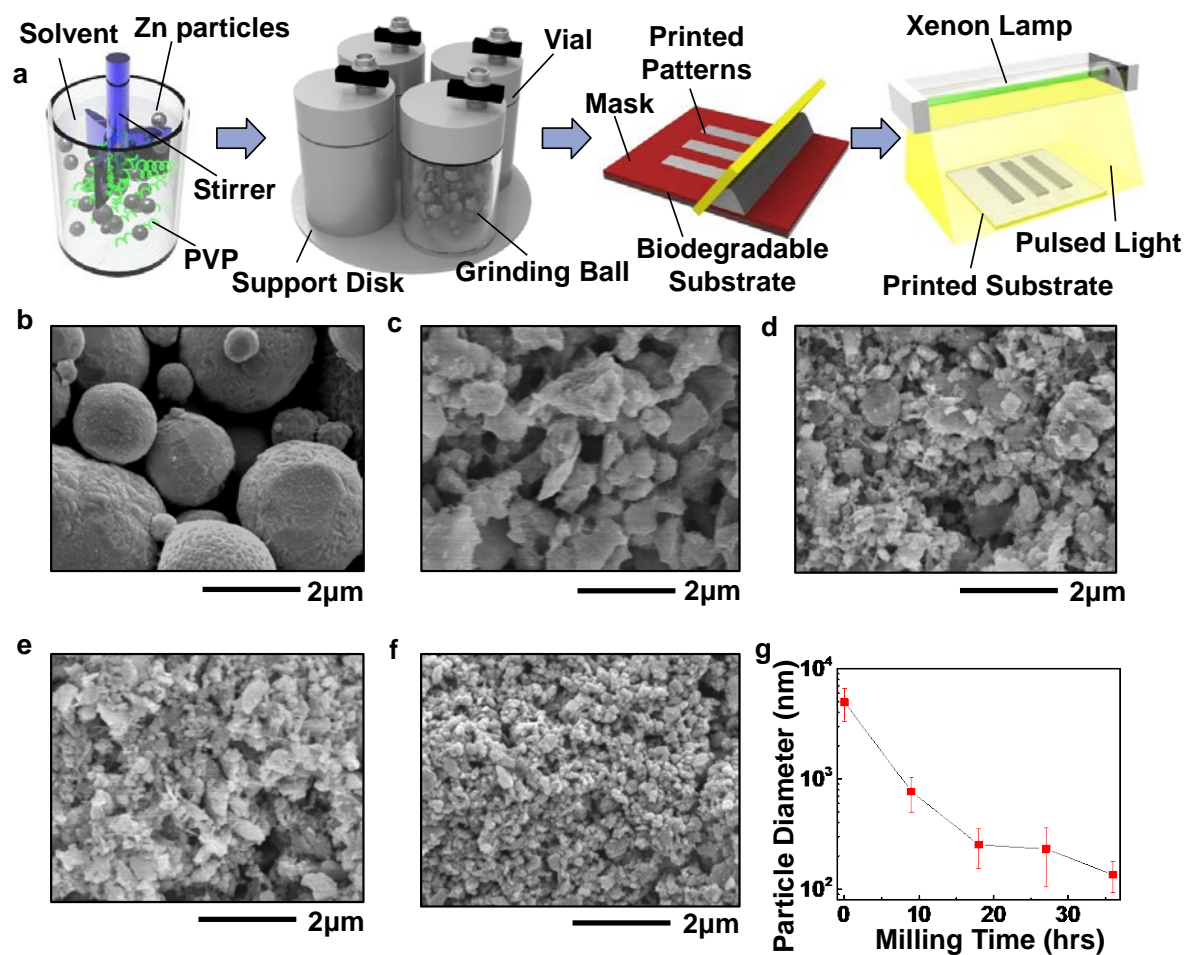


Figure 1. (a) Flow chart of the experiments. Morphology of zinc particles milled for (b) 0 hours (c) 9 hours (d) 18 hours (e) 27 hours and (f) 36 hours. (g) Average particle diameter (as calculated by ImageJ) as a function of milling time.

hours obtained through analyzing the SEM images with ImageJ software using its ‘sharpen’ and ‘threshold function. The diameters of the particles are reduced to ~135 nm after 36 hours of milling from an average size of ~5 μm before the milling. Figure 2a shows the SEM of particles, which was milled in solution containing no PVP but methanol and butyl-acetate only. As comparison, Figure 2b shows the SEM of particle milled in the same solution but with 1 wt% of PVP, in which case excessive PVP is introduced. When zinc

particles are milled with no PVP, they undergo cold welding, leading to agglomerated particles that are even larger than the starting materials. However, excessive amount of PVP (1 wt %) forms thick surface coating around the particles, and increases viscosity of the solution, preventing any further reduction in particle size due to large drag force applied to the milling balls and reduction of impact energy. The results suggest that 0.1 wt% of PVP is an appropriate ratio (Figure 1c), which can lead to effective size reduction of the Zn particles, and, thus, are used throughout the rest of the experiments.

The information on phases, crystal orientations and morphology of Zn NPs can be characterized by X-Ray Diffraction (Figure 2c). The obtained spectra are compared with values from Joint Committee on Powder Diffraction Standards (JCPDS) card for ZnO (JCPDS PDF #036-1451) and Zn (JCPDS PDF #00-004-0831). For the sample milled with 0.1 wt% PVP, diffraction peaks occur at $2\theta = 36.3^\circ$, 39° and 43.3° which corresponds respectively to {002}, {100} and {101} lattice planes of the hexagonal Zn crystal in the space group $P6_3/mmc$, where 'P' stands for primitive Bravais lattice, '6' stands for hexagonal, '3' represents the chirality, and 'mmc' stands for Herman-Mauguin symbols. Other diffraction peaks observed at 28.03° , 25.04° , 21.03° , and 23.03° correspond to {102}, {103}, {110} and {112} lattice planes of Zn metal, respectively. The inter-planar spacing d can be determined using Bragg's law:

$$n\lambda = 2d \sin \theta \quad (1)$$

Where n is a positive integer, λ is the wavelength of the incident wave and θ is the scattering angle. Lattice 'a' and 'c' can be calculated using the standard formula for hexagonal crystal system:

$$\frac{1}{d^2} = \frac{4}{3} \left(\frac{h^2 + hk + k^2}{a^2} \right) + \frac{l^2}{c^2} \quad (2)$$

The lattice constants are found to be $a = b = 2.66193\text{\AA}$ and $c = 0.493716\text{\AA}$ with $\alpha = \beta = 90^\circ$, $\gamma = 120^\circ$. The crystal size, τ , can then be calculated using the Scherrer's formula:

$$\tau = \frac{K\lambda}{\beta \cos \theta} \quad (3)$$

where K is a dimensionless shape factor that is 0.9, λ is the X-ray wavelength, β is the line broadening at half the maximum intensity (FWHM), in radians, and θ is the Bragg angle.

The crystal size of Zn NPs can then be determined to be 34.834 ± 1.76 nm.

ZnO peaks can also be observed on the ball milled samples with and without PVP. The diffraction peaks at 31.8° and 34.46° corresponds respectively to $\{100\}$ and $\{002\}$ lattice planes of the hexagonal ZnO crystal in space group $P6_3/mmc$. The presence of ZnO might be attributed to the reaction between the oxygen atoms in PVP molecule $(C_6H_9NO)_n$ and Zn under milling conditions. In addition, oxygen levels within the glove box where the vials are sealed and leakage of sealed vials can be other possible sources that lead to ZnO within the samples. Although the ball mill is stopped every 5 minutes after continuous running for 15 minutes to prevent heat from building up in the vials, excessive heat generated due to the collision among balls, powders, and the inner wall of the vials during the milling processes may facilitate the reaction between Zn and traces of oxygen and the formation of zinc oxide.

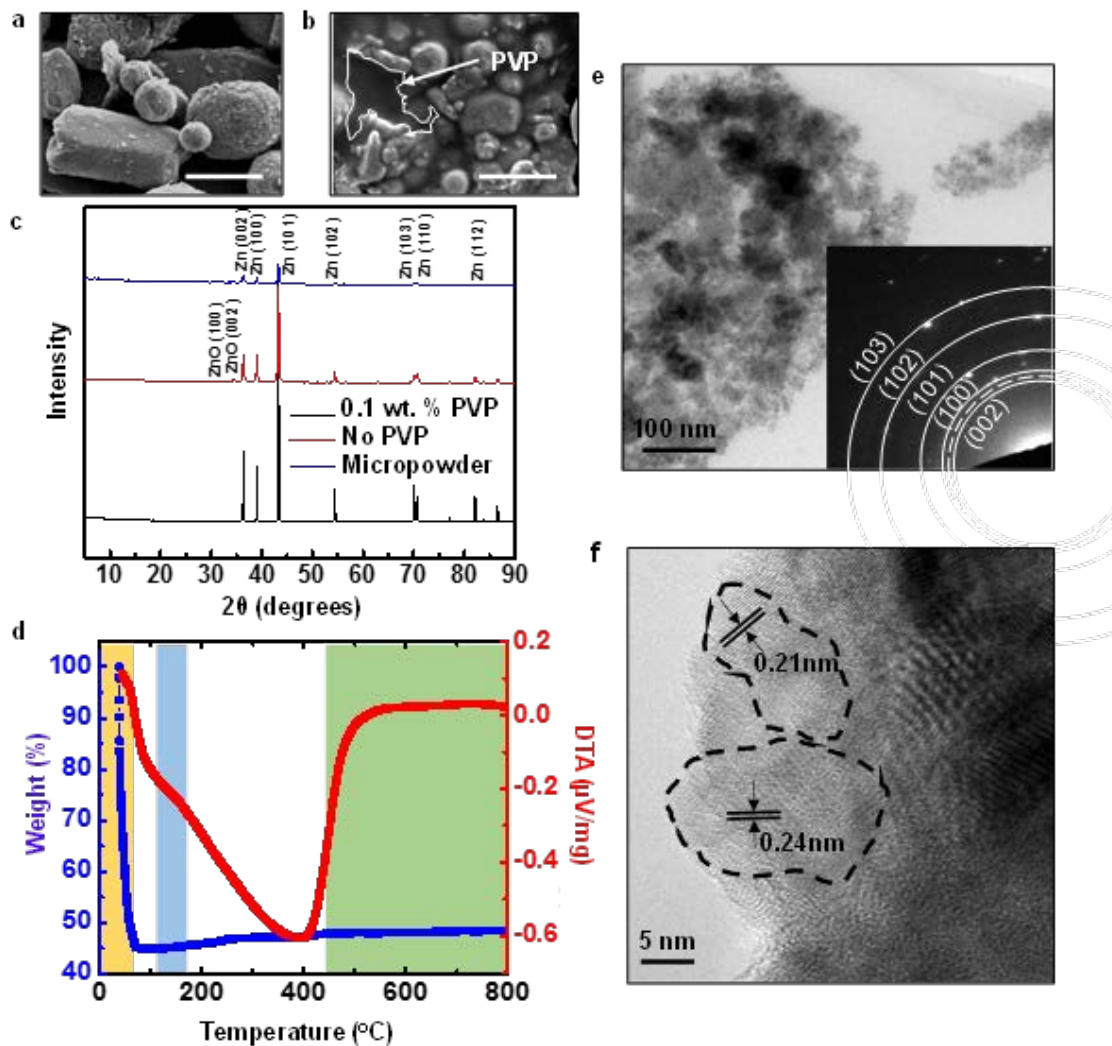


Figure 2. Physical and chemical characterizations of ball milled zinc samples. The scale is of $2\mu\text{m}$ for figure (a) and (b). SEM image of the ball milled sample with (a) No PVP (b) 1 wt % PVP in the solution. (c) XRD spectra of the as received Zn microparticles, samples ball milled for 36 hours with no PVP and 0.1 wt% PVP (d) TG-DTA characterizations of the Zn produced by 36 hours of milling (e) TEM image of the samples ball milled for 36 hours and SAED pattern of the selected area (in inset) (f) HRTEM image of the samples showing crystallite structures with dashed lines.

Thermal characteristics and composition changes of Zn NPs under different temperatures has been examined by TG-DTA. Figure 2d shows that the Zn NPs experience

a distinguished three stages up to 620°C. At the first stage (30°C-90°C) (represented by yellow box), the weight is rapidly decreasing and heat flow is declined as the liquid contents (Methanol and Butyl Acetate) evaporates off the Zn NPs. In the second stage, stage (130°C-180°C, represented by blue box), the PVP layer is degraded. In the third stage (440°C-800°C), represented by green box), shows sintering of Zn NPs and weight gain.

In parallel with the results obtained by XRD, transmission Electron Microscopy (TEM) was conducted to quantify the morphology, size distribution, and grain size of the ball milled samples. The particles sizes as seen from the TEM image varies from ~10nm to ~100nm displaying similar results to those observed by SEM. The high resolution TEM of a fragment of particle shows that the obtained particles are crystalline in nature with a grain size of around 25nm. By analyzing elastic scattering of electrons, information about crystallinity of the milled sample can be obtained. A selected area diffraction pattern (SAED) of the milled sample is shown in inset of Figure 2e, exhibiting scattered bright spots and rings. Careful examination of the rings reveals large number of spots, which might be due to the Bragg reflections of individual crystals, suggesting that the milled zinc is poly nanocrystalline. D-spacing (inter-planar distance) of each set of atomic plane that contributes to diffraction can be calculated from the diameter of the diffraction rings. The diameters (represented in the inset by continuous lines) were found to be of approximately 0.13nm, 0.17nm, 0.21nm, 0.23nm and 0.25nm, respectively, for the first five reflections, corresponding to {103}, {102}, {101}, {100} and {002} lattice planes of the hexagonal Zn crystal according to JCPDS PDF #00-004-0831. The diameter represented by the dashed line was found to be of 0.24nm which corresponds to {101} lattice planes of ZnO according to JCPDS PDF #00-036-1451, indicating the presence of small amount of oxide

in the sample. HRTEM (i.e. large objective-aperture bright field electron phase-contrast) images of Zn nanoparticles formed by 36 hours of milling are shown in Figure 2f. The spacing between the electron diffraction fringes are approximately 0.24nm and 0.21nm, which corresponds respectively to {002} and {101} lattice plane spacing for HCP zinc crystal. The individual crystals (marked by dashed lines) are found to be length ~25-35nm, which is in agreement with the results obtained by XRD.

X-Ray Photoelectron Spectroscopy (XPS) can be used to quantitatively analyzing the composition of Zn NPs. The XPS survey spectra shows the presence of Zn NPs and atoms of C, N and O. No other peaks were found indicating the high purity of the sample. The spectra of C1s has been resolved in two peaks (284.68eV and 287.2 eV). The peaks at 287.2eV and 284.68 can be attributed to C-N and C-H bonds, which may have formed during the process of ball milling. The spectra for O1s has been observed with peaks (530.2 and 531.67), which can be attributed to oxide states of Zn²⁺. The binding energy of 399.28 eV arising from N1s (Figure 3a) is due to C-N complex, which indicates the interaction of Zn nanoparticles and Nitrogen atoms. The binding energies of ZnO and Zn for Zn 2p_{3/2} and Zn 2p_{1/2} are very close to each other and also their chemical shifts (23.1 eV) are same, which makes it difficult to distinguish them. However, referring to similar literatures²⁶, the binding energies were allocated to Zn. The fitted curves and narrow width of the peak indicates that only pure zero-valent zinc is present in the sample, suggesting effective encapsulation of Zn NPs by PVP. Further analysis of the peaks reveals the mass concentrations of Zn 2p, O1s, N1s and C1s, which has been found to be 70.47 %, 14.23%, 1.82% and 13.48 % respectively, indicating that only small amount of the samples has been oxidized.

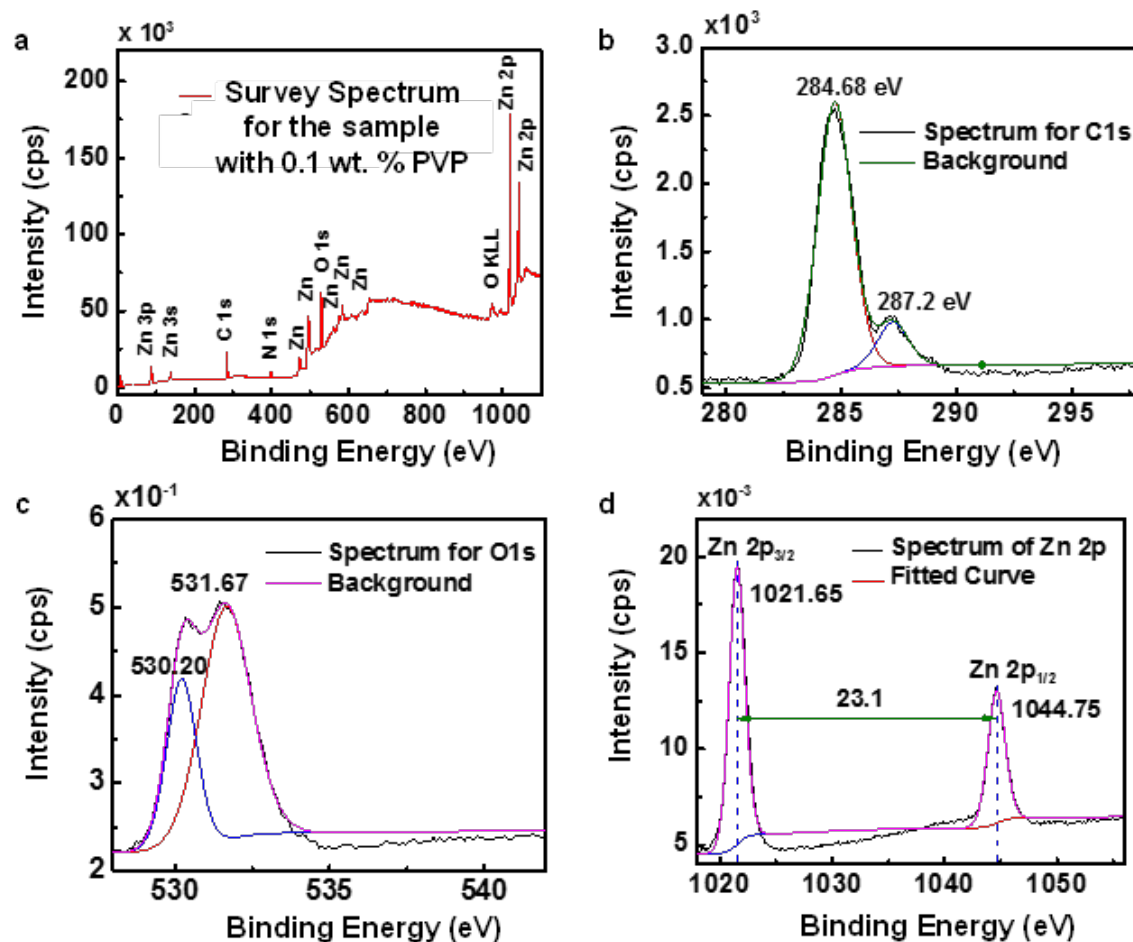


Figure 3. (a) XPS survey spectrum of the sample ball milled for 36 hours. High resolution XPS spectra of (b) carbon (c) oxygen (d) zinc.

The milled Zn NPs can be used to prepare bioresorbable ink, which is stable and well dispersed with negligible precipitate over a period of 4 months (Figure 5a), suggesting the potential use of such ink for printable transient electronics. The printed patterns on bioresorbable substrates can be sintered by a pulsed xenon lamp, which offer 2 ms light pulse at sufficient light intensity and broad spectrum to cause the local heating of Zn NPs

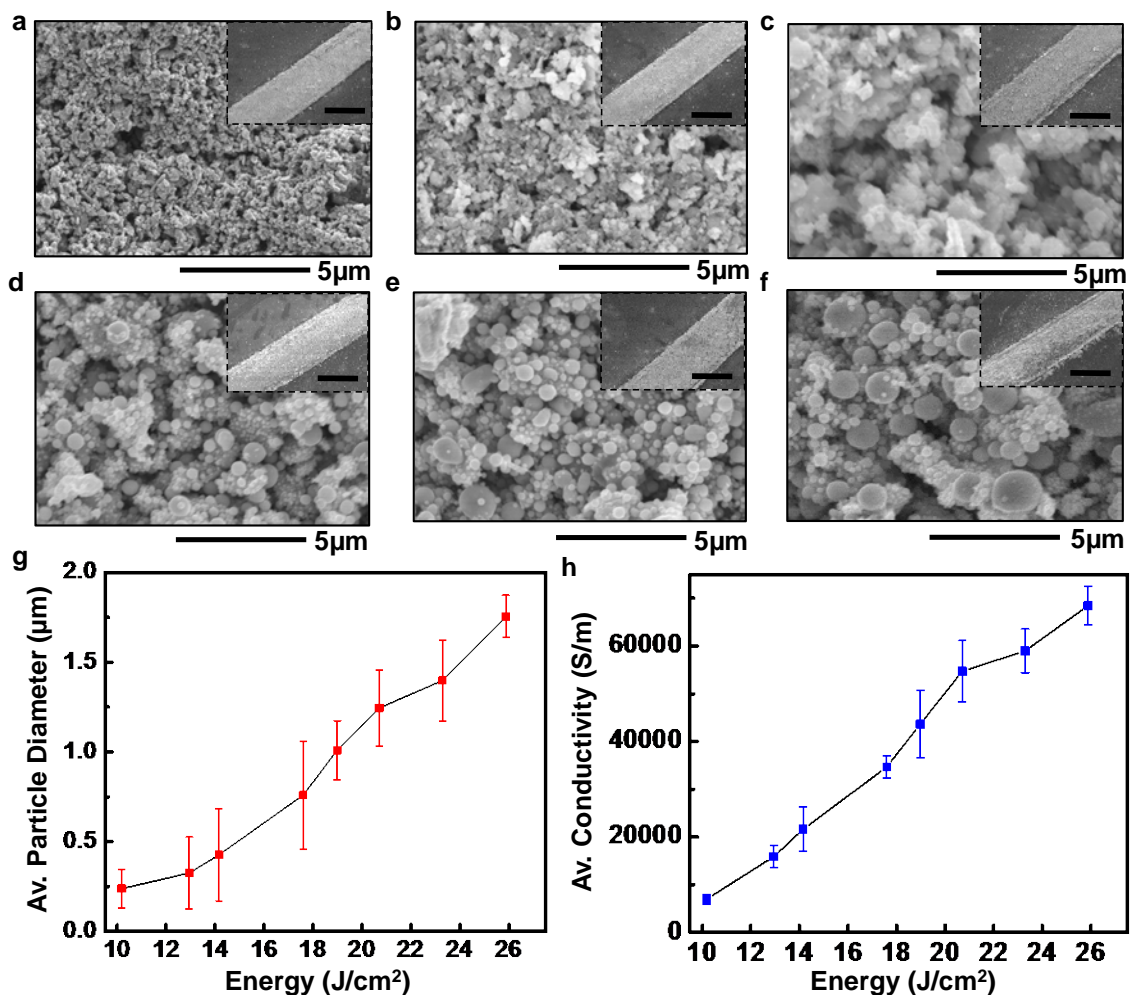


Figure 4. Morphology and characterizations of flash sintered ball milled zinc samples. The scale is of 2μm for all images. The scale is 0.5mm for the images in the inset (a) as deposited samples. Samples flash sintered once at a voltage of (b) 1.8kV (10.18 J/cm²) (c) 2kV (14.15 J/cm²) (d) 2.2 kV (18.98 J/cm²) (e) 2.3 kV (20.7 J/cm²) and (f) 2.5 kV (25.88 J/cm²). (g) Average particle diameter and (h) conductivity as function of increasing energy when subjected to photonic sintering in argon environment.

due to light absorption, leading to the sintering of the printed patterns. The photonic sintering methods are primarily used to sinter nanoparticles such as gold, silver, or copper, and have been presented to sinter bioresorbable inks. Preliminary results shown in Figure 4a to 4f demonstrate the capability of sintering milled Zn NPs with pulsed light, while

systematic research about sintering of bioresorbable nanoparticle ink will be explored in future research. As observed in Figure 4, the average size of nanoparticles increases with increased energy, indicating the effectiveness of particle melting. This effect is pronounced in Figure 4b and 4c. However, as seen in figure 3f, conductivity increases indicating more agglomeration of nanoparticles forming better conductive patterns, with increasing energy. Although the highest conductivity of 72491 S/m was measured at 2.5kV (25.88 J/cm²) of flash, this energy might not be the optimum one for sintering. There is a trade-off between delamination and conductivity obtained. However, instead of forming a continuous film, Zn tends to form spherical shapes (Figures 4d, 4e and 4f) due to its very high surface energy. The images of the printed strips (inset) shows that with increasing energy, more and more delamination occurs, making the measurement unreliable. The strip printed in PVA and Na-CMC dissolves away in water completely in about 3 hours and 12 hours respectively (Figure 5c). Na-CMC is a biocompatible material that have been used for emulsions^{28,29} and thickeners^{30,31}. To achieve good printability, in addition of stability of the inks, the solvent should have low surface tension (γ) to achieve good surface wetting, which requires the surface energy of the printed substrate to exceed the surface tension of the solvent. The surface tension of the solvent i.e., methanol and butyl acetate is 22.7 mJ/m² and 25.1 mJ/m² respectively. The surface energy of Na-CMC is 71mJ/m², thus satisfying the surface wetting condition and hence a perfect material for printing. Moreover as cast Na-CMC has a surface roughness of ~8-9 nm, allowing high quality surface coating. The

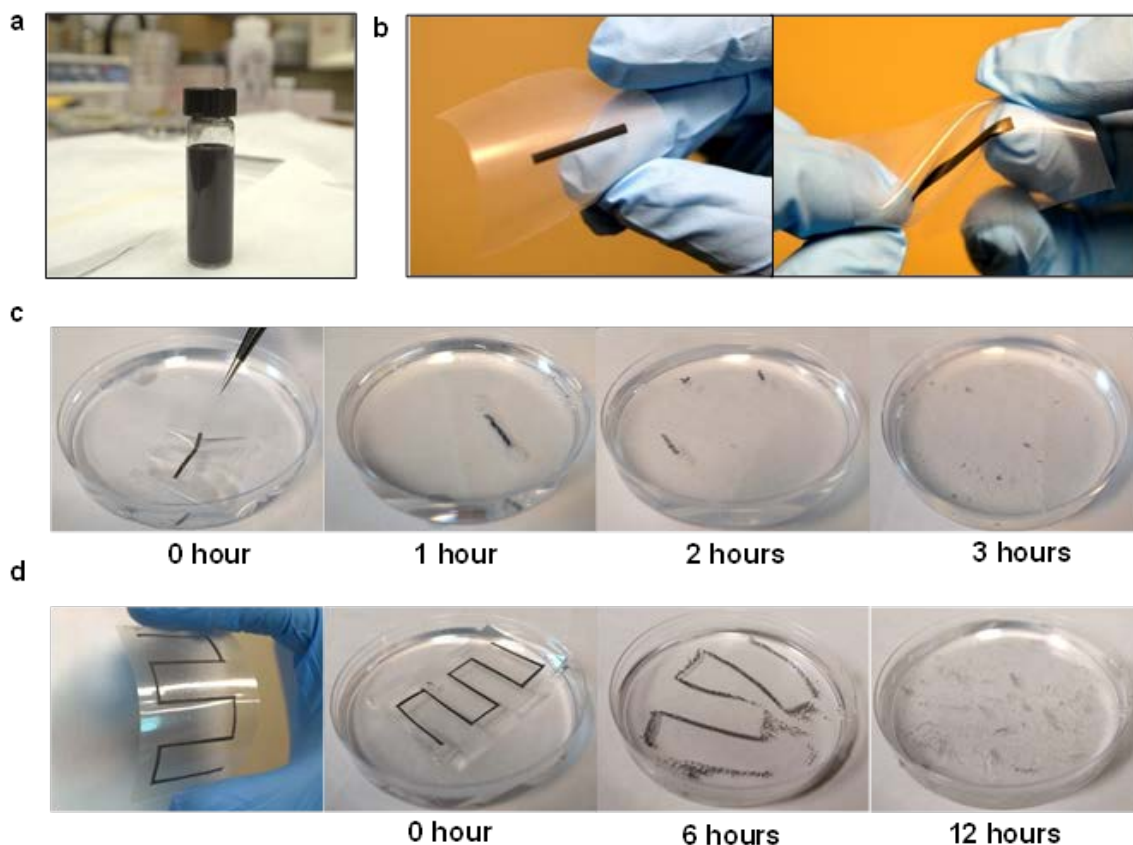


Figure 5. (a) Stable ball milled ink in a glass bottle before printing (b) Pattern printed on a flexible and bendable substrate (c) The pattern dissolving in water in about 3 hours. (d) Pattern dissolving in water in about 12 hours when mounted on Na-CMC substrate.

encapsulation layers and packaging materials such as MgO^7 , SiO_2 , Si_3N_4^8 can be used to control dissolution rates and to protect the printed patterns from humidity. Surface oxide formed on the sintered Zn NPs might be one reason behind low conductance of zinc. This opens a new area of research which will be dedicated to bring up the conductivity of zinc and make it comparable to that of silver, gold or copper NPs. One approach can be improving the surface properties of the bio-degradable substrate, so that it remains immune to high energy flashes and increased adhesion of NPs to the substrate surface. For the Zn

NPs to be used in applications other than printed electronics, the removal of solvent and PVP might become necessary. TG-DTA results shows that by heating the Zn NPs produced by ball milling in Argon environment at maximum of 180°C, all the solvents and PVP can be removed leaving Zn nanopowders, leaving it suitable for any potential application. The printed patterns and the substrates dissolves completely in water within few minutes or hours.

CONCLUSION

In this study, synthesis of poly nano-crystalline zinc has been achieved using ball milling at room temperature, which was previously thought to be impossible. When 0.1 wt% PVP is added to the solvent used in wet milling, it not only prevents cold welding but also successfully aids in producing nanoparticles. The average particle size achieved is 135nm. TEM and XRD analysis provides evidence of crystallinity in the final product. XPS studies reveal that a very small amount of the nanoparticles are oxidized. It also provides confirmation that the particles are stable and encapsulated by PVP. Using this method, high yield of crystalline Zn NPs are possible inexpensively and reliably, which will have tremendous importance in biomedical and other applications. Simple patterns have been printed on different biodegradable substrates which demonstrates that the ink (PVP encapsulated Zn NPs in Methanol and Butyl acetate) can be potentially used in printed electronics which are biodegradable and bioresorbable.

MATERIALS AND METHODS

Ball Milling of Zinc: Zinc micro powders (Sigma Aldrich, St. Louis, MO, USA) with average particle size of $\leq 10 \mu\text{m}$ and purity $\geq 98\%$ were used as milling materials. A solution mixed with 90 wt % of methanol (J.T. Baker) and 10 wt% of Butyl Acetate (99.5% purity, Sigma Aldrich), 0.1 wt. %PVP (Molecular weight: 10000, Sigma Aldrich) were added to the solution under 180 rpm magnetic stirring at 80°C for 30 minutes. The prepared solution along with two kinds of hardened stainless steel balls (Ball type 1: Diameter 3/16 inch, Weight: 0.45g and Ball type 2: Diameter 5/16 inch, Weight: 2.08g) and 8 g of zinc were loaded in a 200ml vial and sealed in Argon environment. The ball-to-powder weight ratio was approximately 20:1 with 63 balls of diameter 3/16" and 63 balls of diameter 5/16". Balls with larger diameters offer high impact force for fracturing, while the balls with smaller diameters provides the grinding force. The amount of filling was about 65% of the volume of the vial. Ball milling was performed in a 4-vial PQ4X series planetary ball mill (PQ4X, Col-Int Tech.) at a rotation speed of 250 rpm throughout the experiments. The milling process lasted for 36 h with 5-minute gaps every 15-minute milling time to reduce temperature buildup in the vial. After milling, the vial was opened in inert atmosphere to nullify any pressure build up.

Water Soluble Substrate Preparation: The bioresorbable substrate used in the experiments were prepared by adding 2wt% Sodium caboxymethyl cellulose (Na-CMC) with water and stirring continuously at 600rpm for 3 hours. The solution was then left to dry for 3-7 days to form a thick, clear, flexible and water soluble film. Kapton tapes of thickness 1mil were used to print patterns with Zn ink of width 400-600 μm and thickness

~0.03 mm. The water soluble substrate used is Polyvinyl Acetate (PVA) which is acquired from Aicello Corporation.

Structure Characterizations: Structures and sizes of the Zn particles were characterized by a scanning electron microscope (Helios NanoLab 600). Transmission electron microscopy was conducted with a FEI Technai F20 FEG-TEM operated at 200kV. The imaging was performed using 5 nm Al₂O₃-coated carbon grid.

Diffraction and Spectroscopy: X-ray diffraction studies were performed using a PANalytical X'Pert Pro Multipurpose Diffractometer using CuK α radiation with a scanning rate of 0.02°s⁻¹. X-ray photoelectron spectroscopy (XPS) was conducted using a Kratos Axis 165 spectrometer. The vacuum level in the chamber remained near 1.0×10^{-8} Torr during the spectra acquisition with a 150 W Aluminum X-ray source.

Thermal Analysis: Thermogravimetric analysis (TGA) and Differential thermal analysis (DTA) were done using NETZSCH STA 409 C equipped with quadrupole mass spectrometer QMS 403 C, with 100mL/min of Argon flow rate and 10°C/min of heating rate.

Photonic Sintering: A photonic sintering system (Sinteron 2000-L), from Xenon corporation with a broadband spectrum of 200-1000 nm, and a xenon lamp, providing the output energy of 0.066-0.22 kJ/in² and a pulse duration of 2 milliseconds, was used to sinter the bioresorbable inks. Photonic sintering was carried out in an aluminum enclosure with a double side polished sapphire wafer, sealed in Argon environment.

ACKNOWLEDGEMENT

The authors would like to thank Dr. Jessica TerBush, Dr. Eric Bohannon and Mr. Brian Porter for help with TEM, XRD and XPS.

REFERENCES

- (1) Gabriel, P.; Rink, L. Zinc and the Immune System of Elderly. *Proc. Nutr. Soc.* **2003**, *59*, 541–552.
- (2) Prasad, A. S. Zinc: An Overview. *Nutrition* **1995**, *11*, 93-99.
- (3) Prasad, A. S. Discovery of Human Zinc Deficiency: 50 Years Later. *J. Trace Elem. Med. Biol.* **2012**, *26*, 66–69.
- (4) Bowen, P. K.; Drelich, J.; Goldman, J. Zinc Exhibits Ideal Physiological Corrosion Behavior for Bioabsorbable Stents. *Adv. Mater.* **2013**, *25*, 2577–2582.
- (5) Zreiqat, H.; Ramaswamy, Y.; Wu, C.; Paschalidis, A.; Lu, Z.; James, B.; Birke, O.; McDonald, M.; Little, D.; Dunstan, C. R. The Incorporation of Strontium and Zinc into a Calcium-Silicon Ceramic for Bone Tissue Engineering. *Biomaterials* **2010**, *31*, 3175–3184.
- (6) Lanocha, N.; Kalisinska, E.; Kosik-Bogacka, D. I.; Budis, H.; Sokolowski, S.; Bohatyrewicz, A.; Lanocha, A. The Effect of Environmental Factors on Concentration of Trace Elements in Hip Joint Bones of Patients after Hip Replacement Surgery. *Ann. Agric. Environ. Med.* **2013**, *20*, 487–493.
- (7) Hwang, S.; Rogers, J. a. A Physically Transient Form of Silicon Electronics. *Science (80-.)*. **2013**, *337*, 1640.
- (8) Hwang, S. W.; Kim, D. H.; Tao, H.; Kim, T. Il; Kim, S.; Yu, K. J.; Panilaitis, B.; Jeong, J. W.; Song, J. K.; Omenetto, F. G.; *et al.* Materials and Fabrication Processes for Transient and Bioresorbable High-Performance Electronics. *Adv. Funct. Mater.* **2013**, *23*, 4087–4093.
- (9) Yin, L.; Huang, X.; Xu, H.; Zhang, Y.; Lam, J.; Cheng, J.; Rogers, J. A. Materials, Designs, and Operational Characteristics for Fully Biodegradable Primary Batteries. *Adv. Mater.* **2014**, *26*, 3879–3884.
- (10) Hwang, S. W.; Huang, X.; Seo, J. H.; Song, J. K.; Kim, S.; Hage-Ali, S.; Chung, H. J.; Tao, H.; Omenetto, F. G.; Ma, Z.; *et al.* Materials for Bioresorbable Radio Frequency Electronics. *Adv. Mater.* **2013**, *25*, 3526–3531.
- (11) Kang, S.; Murphy, R. K. J.; Hwang, S.; Lee, S. M.; Harburg, D. V.; Krueger, N. A.; Shin, J.; Gamble, P.; Cheng, H.; Yu, S.; *et al.* Bioresorbable Silicon Electronic Sensors for the Brain. *Nature* **2016**, *530*, 71–76.
- (12) Rogers, J. A.; Omenetto, F. G.; Hwang, S. W.; TAO, H.; Kim, D. H.; Kaplan, D. Transient Devices Designed to Undergo Programmable Transformations, 2013.

- (13) Lee, C. H.; Kang, S. K.; Salvatore, G. A.; Ma, Y.; Kim, B. H.; Jiang, Y.; Kim, J. S.; Yan, L.; Wie, D. S.; Banks, A.; *et al.* Wireless Microfluidic Systems for Programmed, Functional Transformation of Transient Electronic Devices. *Adv. Funct. Mater.* **2015**, *25*, 5100–5106.
- (14) Huang, X.; Liu, Y.; Hwang, S. W.; Kang, S. K.; Patnaik, D.; Cortes, J. F.; Rogers, J. A. Biodegradable Materials for Multilayer Transient Printed Circuit Boards. *Adv. Mater.* **2014**, *26*, 7371–7377.
- (15) Wegner, K.; Ly, H. C.; Weiss, R. J.; Pratsinis, S. E.; Steinfeld, A. In Situ Formation and Hydrolysis of Zn Nanoparticles for H₂ Production by the 2-Step ZnO/Zn Water-Splitting Thermochemical Cycle. *Int. J. Hydrogen Energy* **2006**, *31*, 55–61.
- (16) Hattori, Y.; Mukasa, S.; Toyota, H.; Inoue, T.; Nomura, S. Synthesis of Zinc and Zinc Oxide Nanoparticles from Zinc Electrode Using Plasma in Liquid. *Mater. Lett.* **2011**, *65*, 188–190.
- (17) Khan, E. H.; Langford, S. C.; Dickinson, J. T.; Boatner, L. A.; Hess, W. P. Photoinduced Formation of Zinc Nanoparticles by UV Laser Irradiation of ZnO. *Langmuir* **2009**, *25*, 1930–1933.
- (18) Guan, Y. F.; Pedraza, a J. Synthesis and Alignment of Zn and ZnO Nanoparticles by Laser-Assisted Chemical Vapor Deposition. *Nanotechnology* **2008**, *19*, 045609.
- (19) Gao, Y.; Hao, J. Electrochemical Synthesis of Zinc Nanoparticles via a Metal-Ligand-Coordinated Vesicle Phase. *J. Phys. Chem. B* **2009**, *113*, 9461–9471.
- (20) Glushenkov, A. M.; Zhang, H. Z.; Chen, Y. Reactive Ball Milling to Produce Nanocrystalline ZnO. *Mater. Lett.* **2008**, *62*, 4047–4049.
- (21) Ozcan, S.; Can, M. M.; Ceylan, A. Single Step Synthesis of Nanocrystalline ZnO via Wet-Milling. *Mater. Lett.* **2010**, *64*, 2447–2449.
- (22) Salah, N.; Habib, S. S.; Khan, Z. H.; Memic, A.; Azam, A.; Alarfaj, E.; Zahed, N.; Al-Hamedi, S. High-Energy Ball Milling Technique for ZnO Nanoparticles as Antibacterial Material. *Int. J. Nanomedicine* **2011**, *6*, 863–869.
- (23) Deng, H. M.; Ding, J.; Shi, Y.; Liu, X. Y.; Wang, J. Ultrafine Zinc Oxide Powders Prepared by Precipitation / Mechanical Milling. *J. Mater. Sci.* **2001**, *36*, 3273–3276.
- (24) Sheibani, S.; Ataie, A.; Heshmati-Manesh, S.; Khayati, G. R. Structural Evolution in Nano-Crystalline Cu Synthesized by High Energy Ball Milling. *Mater. Lett.* **2007**, *61*, 3204–3207.
- (25) Scholz, G.; St, R. Local Structural Orders in Nanostructured Al₂O₃ Prepared by High-Energy Ball Milling. **2002**, *14*, 2101–2117.

- (26) Lin, J.-H.; Patil, R. a; Devan, R. S.; Liu, Z.-A.; Wang, Y.-P.; Ho, C.-H.; Liou, Y.; Ma, Y.-R. Photoluminescence Mechanisms of Metallic Zn Nanospheres, Semiconducting ZnO Nanoballoons, and Metal-Semiconductor Zn/ZnO Nanospheres. *Sci. Rep.* **2014**, *4*, 6967.
- (27) Sinteron 2000-L, Installation and User Manual, Xenon, Corporation. **2013**.
- (28) Diftis, N.; Kiosseoglou, V. Improvement of Emulsifying Properties of Soybean Protein Isolate by Conjugation with Carboxymethyl Cellulose. *Food Chem.* **2003**, *81*, 1–6.
- (29) Adeyeye, M. C.; Jain, A. C.; Ghorab, M. K. M.; Reilly, W. J. Viscoelastic Evaluation of Topical Creams Containing Microcrystalline Cellulose/sodium Carboxymethyl Cellulose as Stabilizer. *AAPS PharmSciTech* **2002**, *3*, E8.
- (30) Pal, K.; Banthia, a K.; Majumdar, D. K. Development of Carboxymethyl Cellulose Acrylate for Various Biomedical Applications. *Biomed. Mater.* **2006**, *1*, 85–91.
- (31) Bayarri, S.; González-Tomás, L.; Costell, E. Viscoelastic Properties of Aqueous and Milk Systems with Carboxymethyl Cellulose. *Food Hydrocoll.* **2009**, *23*, 441–450.

PAPER

II. Photonic Sintering of Bioresorbable Zinc Nanoparticle Ink For Transient Electronics Manufacturing

Bikram K Mahajan,[§] Brandon Ludwig,[§] Wan Shou, Xiaowei Yu, Emmanuel Fregene, Heng Pan,^{} and Xian Huang^{*}*

B.K.Mahajan, B. Ludwig, W.Shou, X.Yu, E. Fregene, Dr. H. Pan

Department of Mechanical Engineering, Missouri University of Science and Technology, Rolla, 65401, USA

Dr. X. Huang

Department of Biomedical Engineering, Tianjin University, Tianjin, 300072, China

*Email: huangxian@tju.edu.cn, hp5c7@mst.edu

§B K Mahajan and B Ludwig equally contributed to this work

ABSTRACT

A new method of manufacturing transient electronics devices is reported. An aerosol printer has been used to print patterns using Zn NPs based bioresorbable ink. The amount of stabilizer and capping agent (PVP) used in the synthesis of the ink was found to be of vital importance during sintering. Lower concentration of PVP results in the formation of surface oxide, while higher concentration of PVP hinders the coalescence of Zn NPs. Resistivity of about 0.1% to that of bulk has been found when 0.1 wt % PVP is used. Analytical simulations has been accompanied with experimental verifications in the study of sintering mechanism of Zn NPs. XPS analysis indicates Zn NP surface protection by PVP. The interface of the conductive pattern and the substrate was studied by EDX. The ink was used to print patterns which can potentially be used as RFID tags, on a

biodegradable Na-CMC substrate. The whole substrate dissolves in water in about 12 hours.

Biocompatible and biodegradable devices have shown promising future in revolutionizing healthcare^[1], consumer electronics^[2] and environmental protection^[3] in past few years. The bioresorbable sensors have potential for in-vivo monitoring of organ^[4], tissue and implants for a pre-decided time and then dissolve in the body, without releasing harmful toxins. The ‘transient electronics’ could be the potential solution of the burgeoning volumes of electronics wastes generated (25 million tons/year) and 82% of which ends in landfills releasing toxic materials such as mercury, lead and brominated flame retardants that pollute the environment. Fully functional printed circuit boards (PCBs)^[2], transistors^[5], energy harvesters^[6], temperature and strain sensors^[7], radio frequency (RF) devices^[8] that dissolves away in a controlled time, have already been demonstrated. However, manufacturing techniques for these devices are based on traditional Complimentary metal-oxide-semiconductor (CMOS) fabrication and surface micro machining methods, requiring expensive and time consuming photolithography, electron beam deposition, and chemical vapor deposition steps^[9]. A typical device may take weeks to fabricate and cost ~\$1000. While mass production can certainly reduce time and cost, current methodologies will never be economically competitive with PCBs, which cost pennies per inch². Therefore developing manufacturing techniques for transient electronics devices using alternative routes which are cheaper, reliable and faster is of incredible importance.

Direct writing or maskless printing, a technique widely used in printed electronics, can be used to deposit functional materials to form scalable patterns on a substrate. They

offer more flexibility, scalability, speed and are relatively cheaper than traditional lithography-based technologies. Inkjet printing (IJP) and aerosol printing (AP) are common direct-writing technologies with IJP being the more documented technology. AP, while being less documented, offers some advantages over IJP when depositing functional liquids. AP allows for more flexible pattern sizes due to the vector based stage system allowing for precise feature dimensions while IJP patterns are more dependent on the drop distance between neighboring droplets (5 μm and higher is common)^[10]. Previously, AP has been used to print devices such as thin-film transistors^[11], current collecting grids for solar cells^[12], radio frequency identification (RFID) tags^[13], strain sensors^[14], and top emitting organic light emitting diodes (OLEDs)^[15].

The AP process starts with atomization of the to-be-deposited ink into 1-5 μm diameter droplets with either a pneumatic or ultrasonic nebulizer. Carrier gas is brought into the system to transport the aerosolized ink to the deposition head. A virtual impactor is incorporated into the system after ink nebulization when a pneumatic nebulizer is used due to the large amount of gas needed for nebulization. The deposition head exit diameter is dependent on the size of the devices to be printed. This printing setup allows for the continuous supply and deposition of functional inks with a wide range of ink viscosities. (0.5 to 2500 cP)^[16]. Working distance between the deposition head and the substrate for AP can be up to 15 mm due to the aerosol stream being focused by the deposition head^[15], A staging system can then be used to mount and move the substrate to obtain the needed feature geometry.

The patterns deposited by AP can be photonically sintered using a xenon lamps, which emits radiation between 200-1200nm. Photonic sintering technique offers various

other unique advantages over other traditional methods, such as furnace heating^[17], selective laser^[18], direct-current^[19], and microwave^[20]. In combination with strategically placed reflectors, high energy densities and thus locally high temperatures enough to sinter the patterns can be achieved, which without the use of very strong power supplies. Using short pulses (2 ms) of optical energy from pulsed xenon light, heat conduction between the inks and the substrates can be minimized to prevent excessive heating and thermal damage to the substrates. Although photonic sintering has not yet been used for sintering bioresorbable inks, several features of the bioresorbable inks including melting point depression and strong photonic absorption suggest great potential in sintering bioresorbable inks through the photonics method.

Here in this report, we demonstrate aerosol printing of patterns using Zn NPs ink, followed by photonic sintering to achieve conductive patterns. Although printing and photonic sintering of materials such as gold (Au)^[21], silver (Ag)^[22] and copper (Cu)^[23] has already been reported extensively, reports on Zn NPs has been rarely been documented before. The high reactivity of Zn NPs coupled with the difficulty to synthesize and handling the particles are few of the reasons. However, our choice of bioresorbable metal is limited to Zinc, Magnesium and Tungsten only. In this report, we develop the recipe of the bioresorbable ink for the best achievable conductivity and aerosol printing in addition to determine photonic sintering parameters for Zn NPs both analytically and experimentally. We also investigate the interface of the printed ink and the substrate which is very important for device performance.

EXPERIMENTAL SECTION

Polyvinylpyrrolidone (Sigma Aldrich, Mw: 10,000) was mixed in a solution of 90 wt% Methanol and 10 wt % butyl Acetate with constant agitation of 200 rpm for 1 hour. Zinc nanopowders (US-nano, 99.9% purity, 65-75nm, metal basis) was mixed with solution and the ink was sonicated for 1 hour before using. Care was taken to keep the temperature of the ink below 30°C while sonication.

The bioresorbable substrate used in the experiments were prepared by adding 2wt% Sodium carboxymethyl cellulose (Na-CMC) with water and stirring continuously at 600rpm for 3 hours. The solution was then left to dry for 6-7 days to form a thick, clear, flexible and water soluble film.

Structures and sizes of the Zn particles were characterized by a scanning electron microscope (Helios NanoLab 600). X-ray photoelectron spectroscopy (XPS) was conducted using a Kratos Axis 165 spectrometer. The vacuum level in the chamber remained near 1.0×10^{-8} Torr during the spectra acquisition. A 150 W Aluminum X-ray source was used and any effects of sample charging were accounted for by fixing the carbon peak. A photonic sintering system (Sinteron 2000-L), from Xenon corporation with a broadband spectrum of 200-1000 nm, and a xenon lamp, providing the output energy of 9.88 J/cm² to 33.33 J/cm² and a pulse duration of 2 milliseconds, was used to sinter the bioresorbable inks. Photonic sintering was carried out in an aluminum enclosure with a double side polished sapphire wafer, sealed in Argon environment.

Aerosol printing was achieved by using a pneumatic nebulizer with nitrogen used to nebulize the ink and to carry the aerosol mist to the deposition head. Mass flow controllers

were used to set the nebulization power and virtual impactor power needed to obtain stable deposition.

DISCUSSION

Figure 1(a) shows a model of a 3-head aerosol printer which was used to print bioresorbable patterns on sodium carboxy-methylcellulose. The substrate was then photonicallly sintered with a xenon lamp to get conductive patterns. Although Au is the best choice due to its stability against oxidation, good electrical conductivity, ease of printing, but Cu is widely used as the raw material is cheap. However, post processing needs to be carried out in a controlled environment to reduce oxidation. In this context, Zn being very reactive^[24], is more prone to oxidation and hence sintering has been carried out in inside an enclosure filled with Argon.

To achieve good printability, in addition of stability of the inks, the solvent should have low surface tension (γ) to achieve good surface wetting, which requires the surface energy of the printed substrate to exceed the surface tension of the solvent^[21]. The surface tension of the solvent i.e., methanol and butyl acetate is 22.7 mJ/m²^[25] and 25.1 mJ/m²^[26] respectively. The surface energy of Na-CMC has been measured as 71mJ/m², thus satisfying the surface wetting condition and hence a compatible material for printing. Moreover as cast Na-CMC has a surface roughness of ~8-9 nm^[2], allowing high quality surface coating. Like every other polymer substrate, Na-CMC has low thermal stability and glass transition temperature in order of 150°C^[27]. When the generated temperature exceed this temperature for a significant amount of time, irreversible damage occurs to the substrate which hampers the device performance. Thus prolonged heating in conventional sintering techniques in out of equation in case of biodegradable substrates. Photonic sintering on the other hand emits multiple pulses of very short duration (2ms), making it

difficult to establish a thermal equilibrium between the substrate and the ink pattern and thus minimizing thermal impact on the substrate and also facilitating R2R production lines^[27]. Additionally, the dark colored Zn NPs have a higher absorbance of radiant energy^[28] than Na-CMC. As a result the local temperature quickly escalates on the as-printed patterns to initiate sintering of the Zn NPs.

The Zn NPs were dispersed in the solvent with a 20% loading. In order to prevent agglomeration, which would result in nozzle clogging or unreliable printing, the NPs are stabilized with amphiphilic molecules like PVP (Molecular weight 10000, in this case) which causes electrostatic and/or electrosteric stabilization and substantially screens the van der Waals attraction between the particles^[28]. Moreover, PVP serves as a binder to assure not only mechanical integrity but also promotes the printability^[29]. However the amount of PVP to be added to the solution has to be doctored carefully. In figure 1(b), as deposited Zn NPs are shown. The solvent (methanol and butyl acetate) evaporated during or after printing, leaving only Zn NPs capped with PVP layers. When sintered, a photochemical reduction takes place and organics (PVP and traces of methanol and butyl acetate) decomposes at around 200°C leaving unprotected NPs behind. With further increase in energy, sintering takes place, resulting in particle growth and particle fusion, which eventually lead to conductivities resembling the bulk metal properties.

In addition to this, as the energy from the flash heats up the particles, it also heats up the substrate beneath and induces melting. The Zn NPs thus get embedded into the

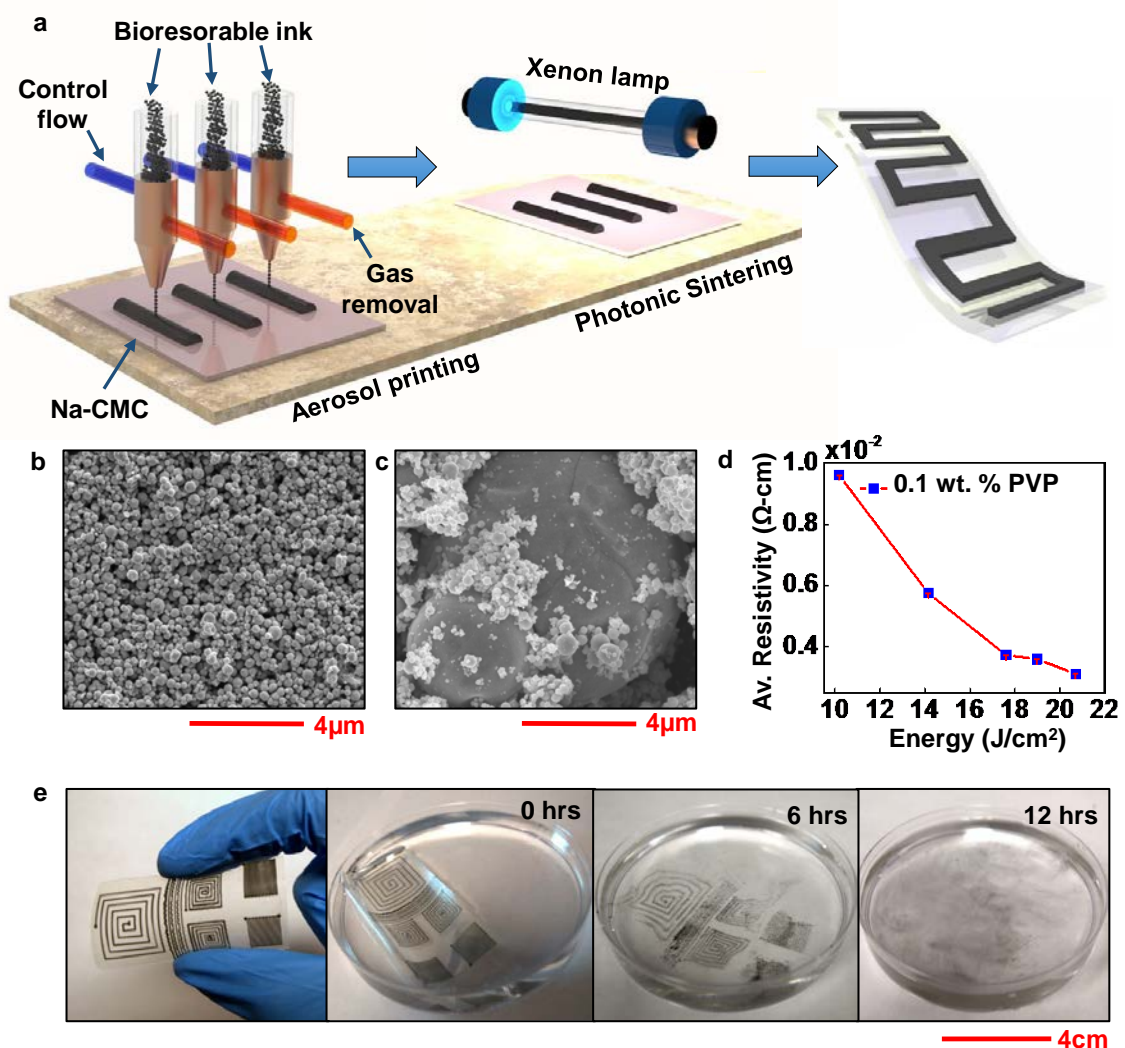


Figure 1. Overview of the new process for transient electronics manufacturing. (a) The set-up for aerosol printing and photonic sintering (b) As deposited Zn nanoparticles with 0.1 wt% PVP (c) Sintered Zn nanoparticles with 1 Flash at $20.7 J/cm^2$. The scale is of $4\mu m$ (d) Resistance study of the sample (e) Transient behavior of the sample.

substrate which promotes adhesion of the printed pattern. While the embedding of Zn into the substrate is beneficial to promote device integrity, too much melting will eventually lead to unreliable device performance. Resistivity decrease with increasing exposed energy

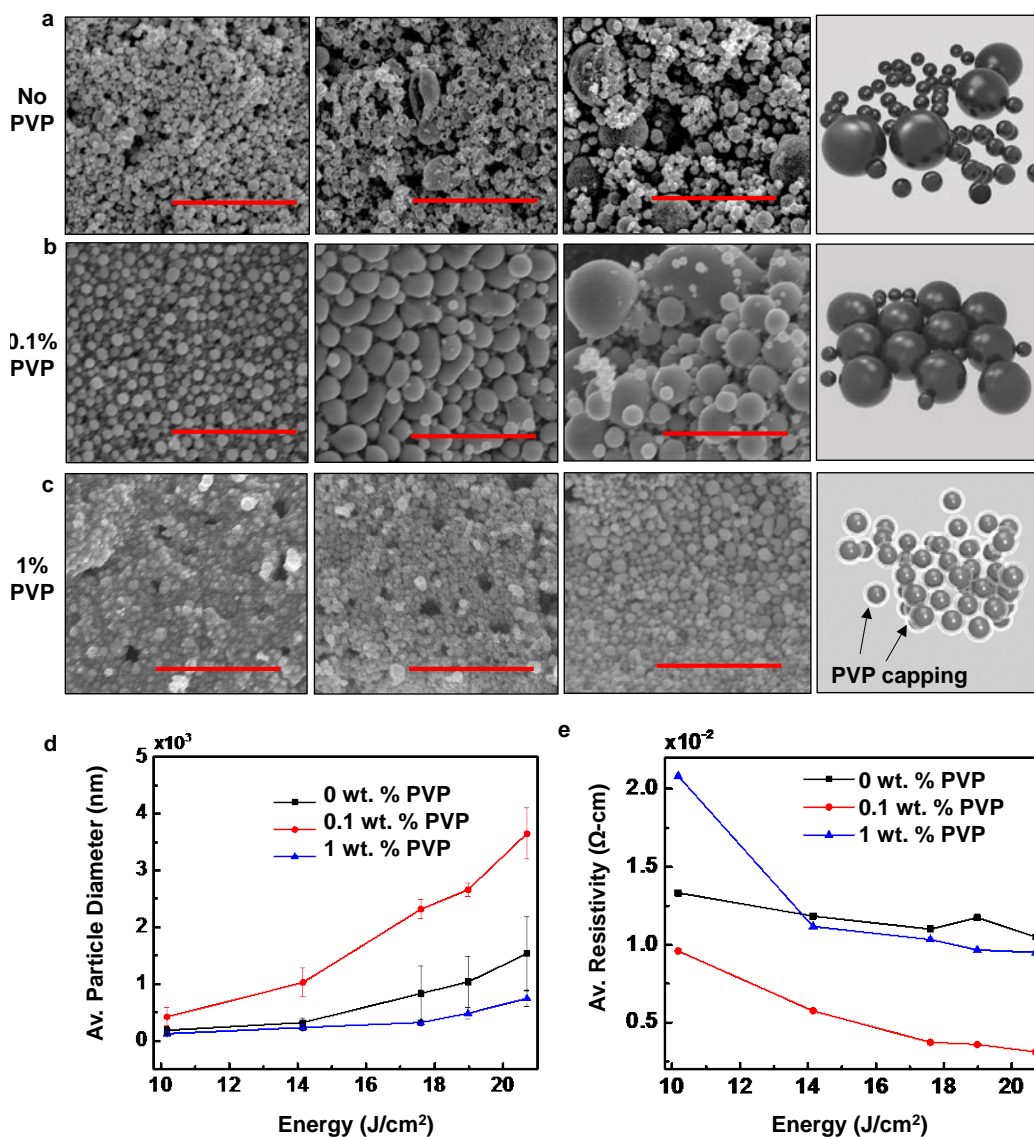


Figure 2. PVP effects on flash annealed structures (in Argon). The mechanism: PVP helps reduce surface zinc oxide to allow coalescence; too much PVP will form matrix that prevents zinc coalescence; too less PVP (high surface oxide) will prevents zinc coalescence. The scale is 5 μ m. Aerosol printed patterns with (a) 0 wt % PVP (b) 0.1 wt % PVP (c) 1 wt% PVP. They were flashed once at 10.18, 17.89 and 20.7 J/cm². The last picture represents the model of the Zn NPS after flashing once at 20.7 J/cm² (d) the average particle diameter with increasing flash voltage. (e) Resistance study of the samples with different PVP concentration.

from photonic sintering as seen in Figure 1(d), reaching as low as $3.3 \times 10^{-3} \Omega\text{-cm}$, which is about 1000 times of the bulk zinc ($5.5 \times 10^{-6} \Omega\text{-cm}$), rendering it usable in printed electronics. One of the primary reasons for high resistivity is oxide layer formation. Figure 1(e) shows an aerosol printed pattern on Na-CMC, which can be used as RFID tags. The printed sample, dissolves completely in water in about 12 hours, when left undisturbed, as shown in Figure 1(e).

The effect of the amount of PVP on sintering is shown in Figure 2 (a, b and c). The sample with no PVP, does show grain growth and coalesce with increasing sintering energy, but is not printable. Although care has been taken to prevent oxidation during the sintering process, Zn NPs being very reactive might pick up oxygen atoms from the solvent and environment to oxidize in ZnO. The sintering temperature of the formed ZnO is significantly higher as compared to Zn and hence it is quite difficult to sinter those particles in a range of temperature where the substrate is not severely affected. Resistivity of $9.8 \times 10^{-3} \Omega\text{-cm}$ has been achieved without any damage of the substrate, which was supposedly from the contribution of the few large Zn beads, which were probably not oxidized.

The situation changes dramatically with the addition of 0.1 wt % PVP. PVP wraps around the Zn NPs and promote better dispersion and resistance to surface oxidation. When sintered, the PVP and traces of other metal organics decompose and coalesce as seen in figure 1(b). This kind of diffusion and possible nanoparticle coalescence phenomena occurs to reach a thermodynamically stable state where the surface area to volume ratio is minimized. However, it needs to be mentioned that the sintering process is accomplished by complete or partial melting. For this reason, the NPs which coalesce to form larger particles during the ink preparation due to its very high surface energy, shows the sintering

effects for which no melting point depression is possible. Although complete removal of organic materials is favorable to achieve high conductivity, it is not absolutely necessary to have NPs to be in contact with each other for sintering. As seen in figure 2(c) concentration of the organic materials is too high and only the top surface is sintered, resulting in low conductivity as seen in figure 2(e). This leads to average particle diameter increase as seen in Figure 2(d) and a resistivity of $1.13 \times 10^{-2} \Omega\text{-cm}$.

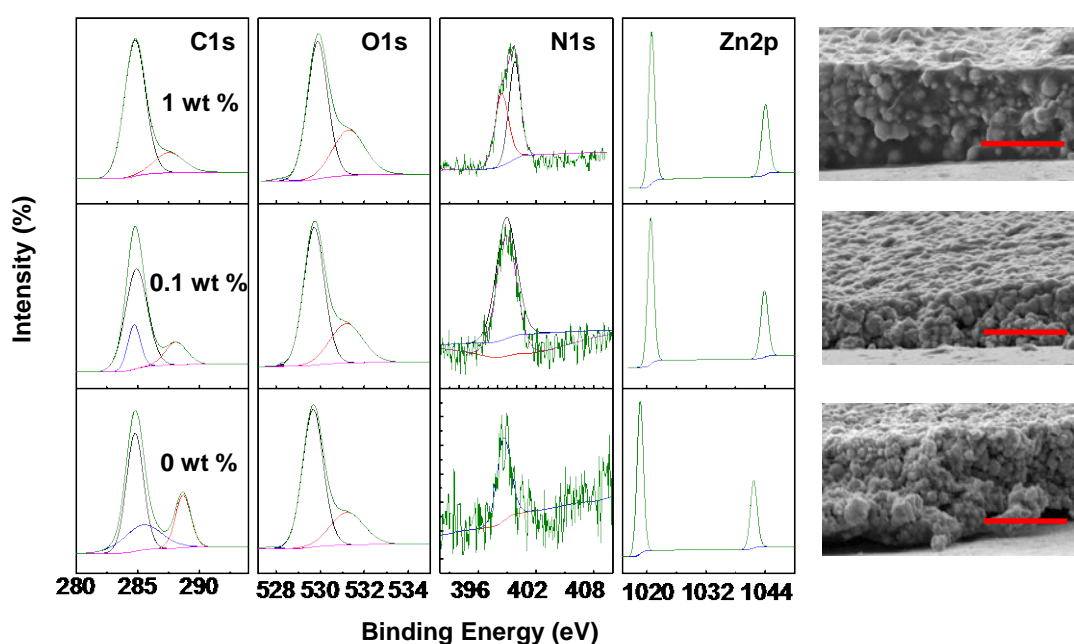


Figure 3. Composition analysis of the annealed Zn in Argon and Ambient. The scale is $2\mu\text{m}$ for the cross-section view of the as-printed aerosol patterns. High resolution XPS spectra of C, N, O and Zn of Zn NPs annealed in argon environment.

To further study the role of PVP, X-ray photoelectron spectroscopy was performed on the samples sintered at 20.7 J/cm^2 , as shown figure (3). The corresponding as deposited samples are also shown in Figure (3). The high-resolution XPS spectra of patterns

containing 0 wt%, 0.1 wt% and 1 wt % PVP are significantly different from each other. The binding energy was referenced to the standard C 1s at 284.8 eV. The XPS survey spectra shows the presence of Zn NPs and atoms of C, N and O. No other peaks were obviously found indicating the high purity of the samples. The Carbon C1s peak has been deconvoluted to 3 peaks at 284.8eV, 286.1eV and 288.4eV for the sample with no PVP which corresponds to C-C (adventitious carbon), -C-O- and -C=O- respectively. While the peak of adventitious carbon is present in all the samples there is a significant change in the -C-O- peak, which almost disappears in the sample containing 1wt% PVP suggesting reduced signal from surface contamination. Also the intensity of -C=O- peaks decreases as the concentration of PVP increases indicating reduced signal from surface contamination.

The oxygen peak has been deconvoluted into 529.88eV and 531.28 eV for the sample containing no PVP, which corresponds to -Zn-O^[31] and -C-O- groups respectively. While -Zn-O- peak is consistent suggesting some degree of oxidation in all samples, the ratio between metal oxides and metal carbonates becomes smaller as higher concentration of PVP is used, indicating surface protection by carbon. The N1s spectra for Zn with 0.1 wt % PVP has been deconvoluted into two peaks at 398.10eV and 399.7eV. The peak at 399.7 has been assigned to C-N units suggesting interaction between N atoms and Zn NPs^[32]. The other peak at 398.2 was assigned to the charged nitrogen atoms. While the peak at 399.7eV remains constant when the amount of PVP is increased, the peak at 398.2eV shifts to 397.5eV suggesting increased interaction between the N atoms and Zn surface. The N1s peak in the sample with no PVP is very weak indicating no such interactions. The binding energies of ZnO and Zn for Zn 2p_{3/2} and Zn 2p_{1/2} are very close

to each other and also their chemical shifts (23.1 eV) are same, which makes it difficult to distinguish them. However, it observed that the Zn2p peaks for the sample containing 0 wt % PVP is around 1018.8 eV and samples containing 0.1 and 1 wt % PVP are at 1020.7eV. This 1.9 eV shift in binding energy indicates that the samples with 0.1 and 1 wt % PVP are much less oxidized than the sample without any PVP^[33], which corroborates with our previous results.

Ambient photonic sintering have used to successfully sinter and achieve good conductivity (greater than 25% of bulk) by reducing CuO NPs dispersed in organic solvent^[34]. However, this process is not suitable of Zn NPs because of the difficulty of finding a suitable reducing agent for highly reactive Zn NPs. Ambient sintering of PVP coated Zn NPs, are also investigated, results of which are given Figure 4(a) and 4(b). To study the sintering mechanism of Zn NPs in air, XPS of the samples containing 0 wt % PVP and 1wt% PVP after being sintered at 20.7 J/cm² is conducted, which is shown in Figure 4(c).

The binding energy was referenced to the standard C 1s at 284.8 eV as in previous case. The XPS survey spectra shows the presence of Zn NPs and atoms of C, N and O. The Carbon C1s peak has been deconvoluted to 3 peaks at 284.8eV, 286.2ev and 289.1eV for the sample with no PVP which corresponds to C-C (adventitious carbon), -C-O- and -C-H- respectively. As the amount of PVP is increased, the -C-O- peak almost disappears, as seen in the case of the samples annealed in Argon environment. The Zn2p peaks are found at 1018.3eV and 1041.4eV. The narrow width suggests that the zinc has been converted into oxide completely in both cases. So, we conclude that, even with very

concentration of PVP, Zn NPs will be oxidized once the organic layer is stripped off due to heating. However, the particles beneath the surface can still be protected from

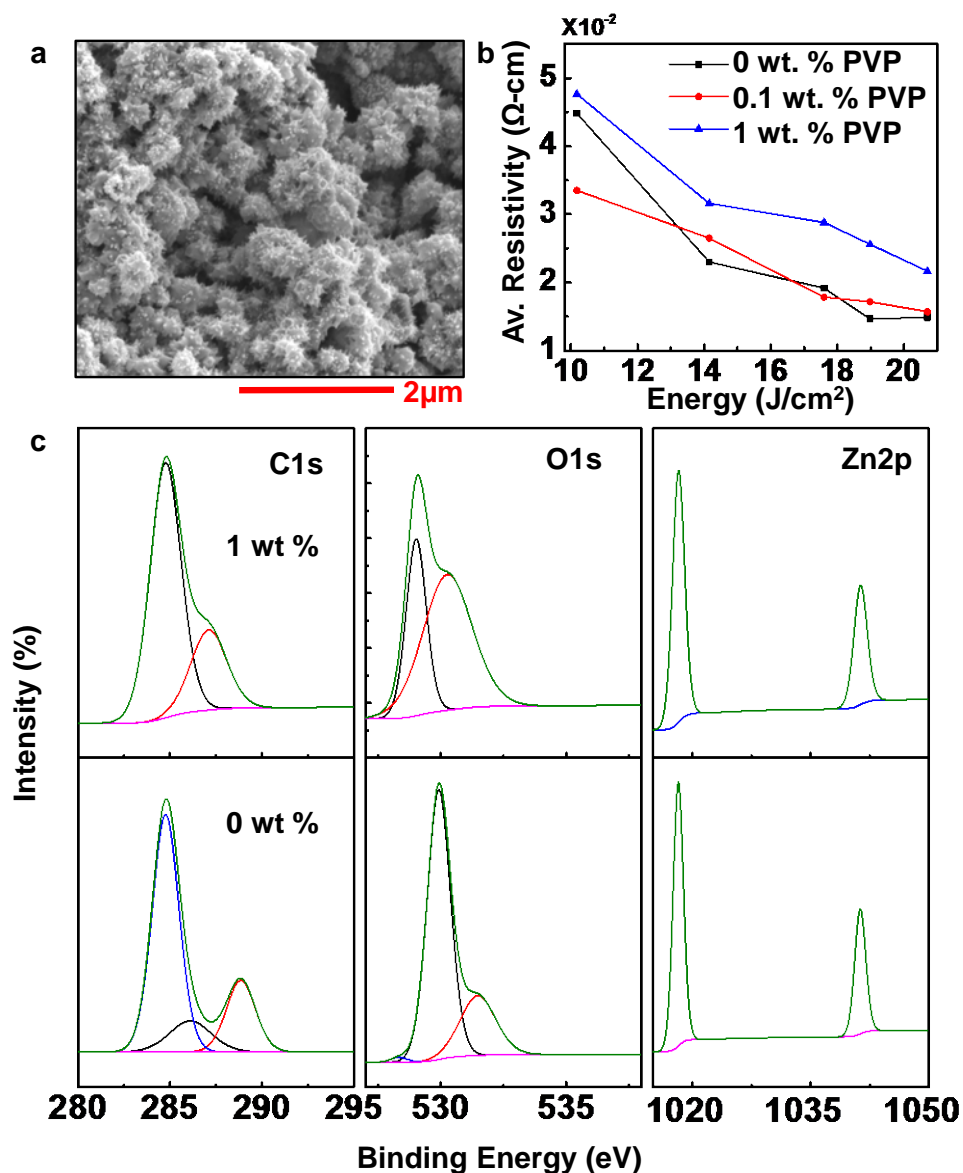


Figure 4. Composition analysis of the annealed Zn in Ambient. (a) Top View of Zn NPs annealed in ambient. (b) Resistivity study of 0 wt% PVP, 0.1 wt% PVP and 1 wt% PVP annealed in ambient. (c) High resolution XPS spectra for C1s, O1s and Zn2p for annealed samples.

environment and coalesce together when subjected to sintering, which is evident from the lowest resistivity of $1.52 \times 10^{-2} \Omega\text{-cm}$ measured from the sample with 0.1 wt % PVP. To understand the transient nanoparticle sintering and coalescence process, rapid melting and solidification of nanoparticles were simulated. The simulation was performed based on numerical solution of mass, energy and momentum conservation equations. The VOF method was used to track the interfaces between nanoparticle and ambient gas. The conservation equation were discretized and the solved using the finite difference method in Fluent, a commercial computational fluid dynamics code. The transient simulation was performed in a 2D $5\mu\text{m} \times 5\mu\text{m}$ computation domain. The domain comprises a 2-3 μm thick layers of Zn NPs on 10 μm thick glass substrate. The Zn NPs layer was initialized using the results from separated Discrete Element Method simulation, wherein Zn NPs depositions and aggregations were simulated. The boundary condition for solving the energy conservation equation is the heat input from the photonic heating pulse. The optical penetration depth of 3 μm was assumed, and incident optical intensity of $9 \times 10^8 \text{ W/m}^2$ was assumed. The optical attenuation and absorption was calculated following Beer's law. The pulse duration was assumed to be 1 μs . The simulated pulse duration is shorter than actual pulse (200-2000 μs) which is mainly limited by computational time. Accordingly, higher optical intensity was used in simulation (actual intensity in experiments $\sim 4 \times 10^7$ to $2 \times 10^8 \text{ W/m}^2$). Despite the shorter pulse used, the simulation was able to provide insight on the coalescence time and effects of nanoparticle film thickness.

The simulation results are presented in Figure. 4. Figure 4(a) represents the condition of the sample before sintering. Nanoparticle films with 1.8 μm and 3.2 μm were prepared and initialized, which is represented in Figure 4(b) and 4(c) respectively. The

same heating pulses were applied on both films. It is found thicker film reaches higher temperature and the film remains in liquid phase for longer period. As a result, the longer

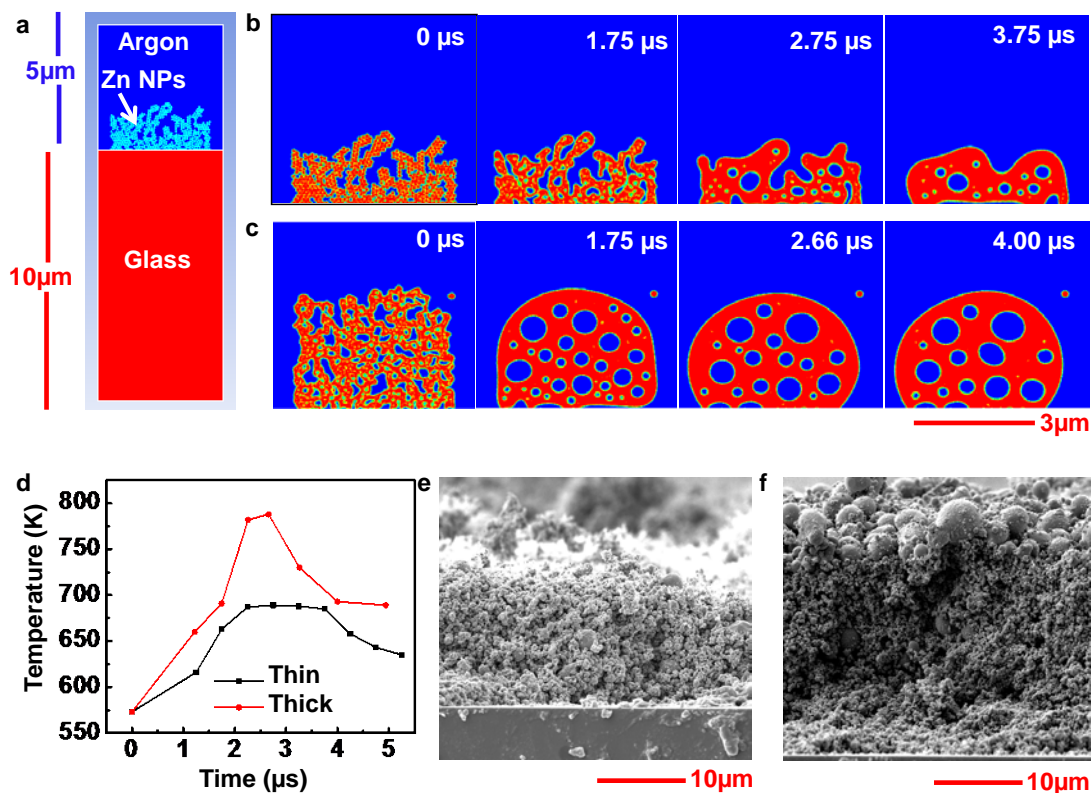


Figure 5. Melting and sintering mechanism and melt depth (simulation and experiments). (a) Generated model comprising of Zn NPs on a 10um glass substrate in Argon environment before heating. Simulation of sintering mechanism (b) thin layer (c) thick layer of Zn NPs in Argon environment at different time interval. (d) Temperature profile for thick and thin layer of Zn NPs generated from simulation. SEM Image of (e) a thin layer and a (f) thick layer of Zn NPs on glass, flashing at 20.7 J/cm^2 .

melt duration completely turns the nanoparticle film into a large spherical droplet before solidified. It is noted several μs melt duration is sufficient to finish the coalescence process driven by surface tension to form 5 μm size beads. Figure 4(d) shows the temperature profile revealing that the thick patterns are locally heated higher than the thin patterns.

To verify the theoretical model, it is necessary that the substrate is not deformed with increasing energy of sintering. However, Na-CMC, having low glass transition temperature, leads to swelling and deformation and hence not ideal for developing the model. Therefore, patterns of different thickness using multiple passes of the aerosol nozzle has been printed on glass and sintered at a 20.7 J/cm^2 at argon environment. As seen in Figure 5(e), Zn NPs might get sintered as coalesce together, but no beading up is observed as seen from the theoretical model. However, Zn NPs coalesce to form beads as big as $7\mu\text{m}$ on the surface when the pattern which is about $30\mu\text{m}$ thick. While the experiments does deviate from the simulation, but the mechanism of sintering can be very well understood. The deviation from simulated model might be due to the presence of surface oxide. Hence, it can be concluded that thickness has a very important role to play.

When sintered at 20.7 J/cm^2 , the dark Zn NPs absorb the light and gets locally heated up. The substrate (glass) on the other hand has very low absorbance of the spectra emitted by the xenon lamp. As a result a strong temperature gradient is created. The thickness of the substrate being about 90 times (glass thickness $\sim 1\text{mm}$) the thickness of the patterns also contributes to the temperature gradient. Even though, the pulse time (2ms) is low, the locally generated temperature is dispersed in case of Figure 5(a). But when the thickness of the pattern is about 30 times to the thickness of the substrate, the gradient is weaker. The locally generated temperature stays on the pattern for a longer time leading to more coalescence. However, there is a bed of Zn NPs beneath the sintered which is left unsintered and thus adding to resistivity.

There are many reports on Au NPs, Ag NPs and Cu NPs, where the whole printed pattern is sintered by photonic sintering, giving a reliable conductance. The reason is that

the NPs undergoes melting point depression with their decreasing particle diameter and hence sintering temperature can be as low as 200°C. According to the Gibbs-Thomson

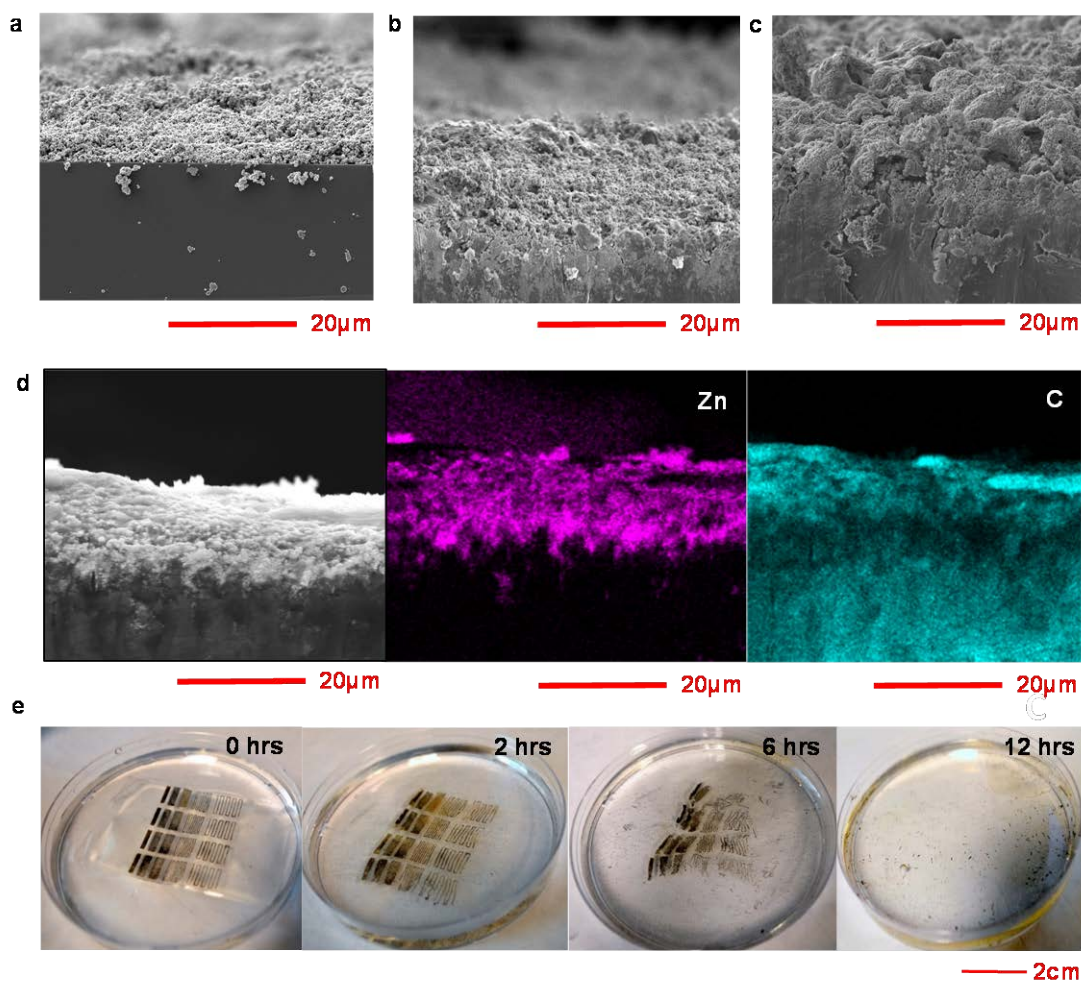


Figure 6. Adhesion study of Zn with Na-CMC and transient behavior. Zn NPs gets into Na-CMC with increasing Flash voltage. (a) as deposited sample (b) 1 Flash at 18.98 J/cm² (c) 1 Flash at 20.7 J/cm². (d) An EDS image is shown at inset where Zn nanostructures getting embedded in the substrate CMC.(e) The substrate fully disappears in about 12 hours.

relation of melting point depression, a depression of only 22°C is obtainable when the particle size is 20nm. For further depression, smaller particle size has to be used, while the

smallest commercially available Zn NPs are of 25nm. The difficulty of obtaining Zn NPs and their stable dispersions in an organic solvent, coupled with very high surface reactivity it is very difficult to achieve melting point depression like Au, Ag or Cu.

Figure 6(a) shows the cross-section of the as-printed Zn NPs on a Na-CMC substrate. As the samples are flashed at high energies, Zn NPs absorbs the light, undergoes melting tends to coalesce, and in the process heating up the top layer of the substrate. Locally generated heat also tends to go into the substrate due to the temperature gradient. As a result, the top surface of Na-CMC substrate melts and solidifies and embedding the Zn NPs in the process. This embedding of Zn NPs in to the Na-CMC increases with the flashing energy as seen in figure 6(c). An EDX image is shown in the inset of figure 6(c), which shows that is is getting embedded into the substrate. Despite increasing the resistivity, embedding is desirable to an extent that helps the adhesion of Zn to the substrate surface, thus combating the delamination which is one of the most common reasons for device failure in printed electronics. Figure 6(d) shows the picture of some resistances printed on Na-CMC using AP. The sample dissolves in water in about 8 hours.

CONCLUSION

In conclusion, a new method of manufacturing transient electronics devices is developed. Instead of using the traditional micromaching and CMOS fabrication techniques aerosol printing is used to p patterns with bio-resorbable Zn ink. The ink was converted into conductive patterns by photonic sintering. Sintering mechanism of Zn NPs has been systematically studied with analytical modelling and experimental verifications. It has been found that the amount of the organic stabilizer (here PVP) has a pivotal role to play in the coalescence of Zn NPs. Although the best resistivity obtained for Zn NPs

reliable is around 0.1% to that bulk Zn, it opens a new dimension of research in using Zn as a bioresorbable ink in printed electronics. The RFID tags printed by ink on a biodegradable Na-CMC substrate dissolves away in water in about 12 hours.

ACKNOWLEDGEMENT

The authors thank Mr. Brian Porter for help with XPS measurements.

REFERENCES

- [1] X. Huang, Y. Liu, H. Cheng, W. J. Shin, J. A. Fan, Z. Liu, C. J. Lu, G. W. Kong, K. Chen, D. Patnaik, S. H. Lee, S. Hage-Ali, Y. Huang, J. A. Rogers, *Adv. Funct. Mater.* **2014**, *24*, 3846.
- [2] X. Huang, Y. Liu, S. W. Hwang, S. K. Kang, D. Patnaik, J. F. Cortes, J. A. Rogers, *Adv. Mater.* **2014**, *26*, 7371.
- [3] S. Hwang, J. a. Rogers, *Science (80-.)*. **2013**, *337*, 1640.
- [4] S. Kang, R. K. J. Murphy, S. Hwang, S. M. Lee, D. V. Harburg, N. A. Krueger, J. Shin, P. Gamble, H. Cheng, S. Yu, Z. Liu, J. G. McCall, M. Stephen, H. Ying, J. Kim, G. Park, R. C. Webb, C. H. Lee, S. Chung, D. S. Wie, A. D. Gujar, B. Vemulapalli, A. H. Kim, K.-M. Lee, J. Cheng, Y. Huang, S. H. Lee, P. V. Braun, W. Z. Ray, J. A. Rogers, *Nature* **2016**, *530*, 71.
- [5] L. Yin, H. Cheng, S. Mao, R. Haasch, Y. Liu, X. Xie, S. W. Hwang, H. Jain, S. K. Kang, Y. Su, R. Li, Y. Huang, J. A. Rogers, *Adv. Funct. Mater.* **2014**, *24*, 645.
- [6] C. Dagdeviren, S. W. Hwang, Y. Su, S. Kim, H. Cheng, O. Gur, R. Haney, F. G. Omenetto, Y. Huang, J. A. Rogers, *Small* **2013**, *9*, 3398.
- [7] J. A. R. Dae-Hyeong Kim^{1,*}, Nanshu Lu^{1,*}, Rui Ma^{2,*}, Yun-Soung Kim¹, Rak-Hwan Kim¹, Shuodao Wang³, Jian Wu³, Sang Min Won¹, Hu Tao⁴, Ahmad Islam¹, Ki Jun Yu¹, Tae-il Kim¹, Raheed Chowdhury², Ming Ying¹, Lizhi Xu¹, Ming Li³, 6, Hyun-Joong Chung¹, Hohyun Keum¹, Marti, *Science (80-.)*. **2011**, *333*, 838.
- [8] S. W. Hwang, S. K. Kang, X. Huang, M. A. Brenckle, F. G. Omenetto, J. A. Rogers, *Adv. Mater.* **2015**, *27*, 47.
- [9] C. H. Lee, S. K. Kang, G. A. Salvatore, Y. Ma, B. H. Kim, Y. Jiang, J. S. Kim, L. Yan, D. S. Wie, A. Banks, S. J. Oh, X. Feng, Y. Huang, G. Troester, J. A. Rogers, *Adv. Funct. Mater.* **2015**, *25*, 5100.

- [10] T. Seifert, E. Sowade, F. Roscher, M. Wiemer, T. Gessner, R. R. Baumann, *Ind. Eng. Chem. Res.* **2015**, *54*, 769.
- [11] C. S. Jones, X. Lu, M. Renn, M. Stroder, W. S. Shih, *Microelectron. Eng.* **2010**, *87*, 434.
- [12] P. Kopola, B. Zimmermann, A. Filipovic, H. F. Schleiermacher, J. Greulich, S. Rousu, J. Hast, R. Myllylä, U. Würfel, *Sol. Energy Mater. Sol. Cells* **2012**, *107*, 252.
- [13] B. L. Xu, Y. Zhao, L. K. Yu, B. Xu, H. E. Zhang, W. L. Lv, D. H. Sun, *Key Eng. Mater.* **2013**, 562-565, 1417.
- [14] D. Zhao, T. Liu, M. Zhang, R. Liang, B. Wang, *Smart Mater. Struct.* **2012**, *21*, 115008.
- [15] J. G. Tait, E. Witkowska, M. Hirade, T. H. Ke, P. E. Malinowski, S. Steudel, C. Adachi, P. Heremans, *Org. Electron. physics, Mater. Appl.* **2015**, *22*, 40.
- [16] J. M. Hoey, A. Lutfurakhmanov, D. L. Schulz, I. S. Akhatov, *J. Nanotechnol.* **2012**, *2012*, DOI 10.1155/2012/324380.
- [17] B. J. Perelaer, A. W. M. de Laat, C. E. Hendriks, U. S. Schubert, *J. Mater. Chem.* **2008**, *18*, 3209.
- [18] I. Theodorakos, F. Zacharatos, R. Geremia, D. Karnakis, I. Zergioti, *Appl. Surf. Sci.* **2015**, *336*, 157.
- [19] M. Hummelgård, R. Zhang, H. E. Nilsson, H. Olin, *PLoS One* **2011**, *6*, 1.
- [20] J. Perelaer, B. J. De Gans, U. S. Schubert, *Adv. Mater.* **2006**, *18*, 2101.
- [21] T. Kraus, L. Malaquin, H. Schmid, W. Riess, N. D. Spencer, H. Wolf, *Nat Nano* **2007**, *2*, 570.
- [22] H.-H. Lee, K.-S. Chou, K.-C. Huang, *Nanotechnology* **2005**, *16*, 2436.
- [23] S. Jeong, K. Woo, D. Kim, S. Lim, J. S. Kim, H. Shin, Y. Xia, J. Moon, *Adv. Funct. Mater.* **2008**, *18*, 679.
- [24] R. D. Rieke, *J. Org. Chem. Commun.* **1981**, 4323.
- [25] M. Wu, T. Cubaud, C. M. Ho, *Phys. Fluids* **2004**, *16*, 2.
- [26] E. J. Chibowski, *Adv. Colloid Interface Sci.* **2005**, *113*, 121.
- [27] S. Wünscher, R. Abbel, J. Perelaer, U. S. Schubert, *J. Mater. Chem. C* **2014**, *2*, 10232.
- [28] J. Perelaer, U. S. Schubert, *J. Mater. Res.* **2013**, *28*, 564.

- [29] S. H. Park, H. S. Kim, *Thin Solid Films* **2014**, 550, 575.
- [30] M. Zenou, O. Ermak, A. Saar, Z. Kotler, *J. Phys. D. Appl. Phys.* **2014**, 47, 025501.
- [31] J. Haber, J. Stoch, L. Ungier, *J. Electron Spectros. Relat. Phenomena* **1976**, 9, 459.
- [32] Z. Zhang, X. Zhang, Z. Xin, M. Deng, Y. Wen, Y. Song, *Nanotechnology* **2011**, 22, 425601.
- [33] S. Bang, S. Lee, Y. Ko, J. Park, S. Shin, H. Seo, H. Jeon, *Nanoscale Res. Lett.* **2012**, 7, 290.
- [34] F. Paglia, D. Vak, J. Van Embden, A. S. R. Chesman, A. Martucci, J. J. Jasieniak, E. Della Gaspera, *ACS Appl. Mater. Interfaces* **2015**, 7, 25473.

SECTION

3. CONCLUSIONS

Zinc is an important trace element which assists in various activities in human body and also is also degradable in bio-fluids. However, Zinc is very reactive and hence very difficult and expensive to synthesize. The goal of this research is to achieve Zinc nanoparticles in a cheap, reliable way which is also safe, high yielding and can be obtained in room temperature. A planetary ball mill, without any modification was used to synthesize Zinc Nanoparticles by milling zinc micro-particles in a solution of methanol and butyl acetate with 0.1 wt% PVP. The weight percent of PVP plays a very important role in the synthesis of nanoparticles. If the amount is less, the Zinc would aggregate via cold welding. If the amount of PVP is more, it would form a viscous solution and hinder the grinding process. The obtained nanoparticles were then characterized using SEM, TEM and surface analysis techniques like XRD and XPS and it was concluded that, the obtained nanoparticles were mostly Zinc with very little oxidation. The obtained particles were directly used to print simple patterns on PVA and Na-CMC, which were then photonicallly sintered using a Xenon Lamp to render them conductive. The patterns dissolves away completely in water showing transient behavior. The scope of the second paper is to do advanced study of the photonic sintering of Zinc nanoparticles. It was found that the amount of PVP is important in the sintering of Zinc. A simulation was done in Fluent to study the mechanism of sintering in thin and thick patterns. It was also observed that while sintering Zinc gets embedded into the substrates promoting adhesion. The lowest resistivity of zinc nanoparticles was found to be about 0.1% to that of bulk zinc.

REFERENCES

- [1] S. T. Tan, B. J. Chen, X. W. Sun, W. J. Fan, H. S. Kwok, X. H. Zhang, and S. J. Chua, "Blueshift of optical band gap in ZnO thin films grown by metal-organic chemical-vapor deposition," *J. Appl. Phys.*, vol. 98, no. 1, 2005.
- [2] Ü. Özgür, Y. I. Alivov, C. Liu, A. Teke, M. A. Reshchikov, S. Doğan, V. Avrutin, S. J. Cho, and H. Morkoç, "A comprehensive review of ZnO materials and devices," *J. Appl. Phys.*, vol. 98, no. 4, pp. 1–103, 2005.
- [3] W.-Y. Chang, Y.-C. Lai, T.-B. Wu, S.-F. Wang, F. Chen, and M.-J. Tsai, "Unipolar resistive switching characteristics of ZnO thin films for nonvolatile memory applications," *Appl. Phys. Lett.*, vol. 92, no. 2, p. 022110, 2008.
- [4] M. Saito and S. Fujihara, "Large photocurrent generation in dye-sensitized ZnO solar cells," *Energy Environ. Sci.*, vol. 1, no. 2, p. 280, 2008.
- [5] J. H. Lim, C. K. Kong, K. K. Kim, I. K. Park, D. K. Hwang, and S. J. Park, "UV electroluminescence emission from ZnO light-emitting diodes grown by high-temperature radiofrequency sputtering," *Adv. Mater.*, vol. 18, no. 20, pp. 2720–2724, 2006.
- [6] S. Liang, H. Sheng, Y. Liu, Z. Huo, Y. Lu, and H. Shen, "ZnO Schottky ultraviolet photodetectors," *J. Cryst. Growth*, vol. 225, no. 2–4, pp. 110–113, 2001.
- [7] Q. Wan, Q. H. Li, Y. J. Chen, T. H. Wang, X. L. He, J. P. Li, and C. L. Lin, "Fabrication and ethanol sensing characteristics of ZnO nanowire gas sensors," *Appl. Phys. Lett.*, vol. 84, no. 18, pp. 3654–3656, 2004.
- [8] L. Wang, X. Li, Y. Zheng, X. Li, W. Dong, W. Tang, B. Chen, C. Li, T. Zhang, and W. Xu, "Nanostructured porous ZnO film with enhanced photocatalytic activity," *Thin Solid Films*, vol. 519, no. 16, pp. 5673–5678, 2011.
- [9] V. Sharma, R. K. Shukla, N. Saxena, D. Parmar, M. Das, and A. Dhawan, "DNA damaging potential of zinc oxide nanoparticles in human epidermal cells," *Toxicol. Lett.*, vol. 185, no. 3, pp. 211–218, 2009.
- [10] R. C. McGlennen, "Miniaturization technologies for molecular diagnostics," *Clin. Chem.*, vol. 47, no. 3, pp. 393–402, 2001.
- [11] J. An, S. Geib, and N. Rosi, "Cation-Triggered Drug Release from a Porous Zinc–Adeninate Metal–Organic Framework," *J. Am. Chem. Soc.*, pp. 8376–8377, 2009.

- [12] S. Das, A. Chaudhury, and K. Y. Ng, "Preparation and evaluation of zinc-pectin-chitosan composite particles for drug delivery to the colon: Role of chitosan in modifying in vitro and in vivo drug release," *Int. J. Pharm.*, vol. 406, no. 1–2, pp. 11–20, 2011.
- [13] A. C. Jamieson, J. C. Miller, and C. O. Pabo, "Drug discovery with engineered zinc-finger proteins," *Nat. Rev. Drug Discov.*, vol. 2, no. 5, pp. 361–368, 2003.
- [14] J. Wang, G. Wang, and J. Zhao, "Nonmetal-metal transition in Zn_n (n=2–20) clusters," *Phys. Rev. A*, vol. 68, p. 5, 2003.
- [15] S. M. Gawish, H. Avci, a M. Ramadan, S. Mosleh, R. Monticello, F. Breidt, and R. Kotek, "Properties of antibacterial polypropylene/nanometal composite fibers.," *J. Biomater. Sci. Polym. Ed.*, vol. 23, no. 1–4, pp. 43–61, 2012.
- [16] a. a. Revina, E. V. Oksentyuk, and a. a. Fenin, "Synthesis and properties of zinc nanoparticles: The role and prospects of radiation chemistry in the development of modern nanotechnology," *Prot. Met.*, vol. 43, no. 6, pp. 554–559, 2007.
- [17] M. Song, M. Chen, and Z. Zhang, "Effect of Zn powders on the thermal decomposition of ammonium perchlorate," *Propellants, Explos. Pyrotech.*, vol. 33, no. 4, pp. 261–265, 2008.
- [18] G. Wu, L. Gong, K. Feng, S. Wu, Y. Zhao, and P. K. Chu, "Rapid degradation of biomedical magnesium induced by zinc ion implantation," *Mater. Lett.*, vol. 65, no. 4, pp. 661–663, 2011.
- [19] C. M. Monteiro, A. P. G. C. Marques, P. M. L. Castro, and F. X. Malcata, "Characterization of *Desmodesmus pleiomorphus* isolated from a heavy metal-contaminated site: Biosorption of zinc," *Biodegradation*, vol. 20, no. 5, pp. 629–641, 2009.
- [20] L. Yin, H. Cheng, S. Mao, R. Haasch, Y. Liu, X. Xie, S. W. Hwang, H. Jain, S. K. Kang, Y. Su, R. Li, Y. Huang, and J. A. Rogers, "Dissolvable metals for transient electronics," *Adv. Funct. Mater.*, vol. 24, no. 5, pp. 645–658, 2014.
- [21] S. W. Hwang, J. K. Song, X. Huang, H. Cheng, S. K. Kang, B. H. Kim, J. H. Kim, S. Yu, Y. Huang, and J. A. Rogers, "High-performance biodegradable/transient electronics on biodegradable polymers," *Adv. Mater.*, vol. 26, no. 23, pp. 3905–3911, 2014.
- [22] X. Huang, Y. Liu, S. W. Hwang, S. K. Kang, D. Patnaik, J. F. Cortes, and J. A. Rogers, "Biodegradable materials for multilayer transient printed circuit boards," *Adv. Mater.*, vol. 26, no. 43, pp. 7371–7377, 2014.

- [23] Y. Gao and J. Hao, "Electrochemical synthesis of zinc nanoparticles via a metal-ligand-coordinated vesicle phase.," *J. Phys. Chem. B*, vol. 113, no. 28, pp. 9461–9471, 2009.
- [24] E. H. Khan, S. C. Langford, J. T. Dickinson, L. A. Boatner, and W. P. Hess, "Photoinduced formation of zinc nanoparticles by UV laser irradiation of ZnO," *Langmuir*, vol. 25, no. 4, pp. 1930–1933, 2009.
- [25] S. C. Singh and R. Gopal, "Zinc nanoparticles in solution by laser ablation technique," *Bull. Mater. Sci.*, vol. 30, no. 3, pp. 291–293, 2007.
- [26] S. C. Singh, R. K. Swarnkar, and R. Gopal, "Zn/ZnO core/shell nanoparticles synthesized by laser ablation in aqueous environment: Optical and structural characterizations," *Bull. Mater. Sci.*, vol. 33, no. 1, pp. 21–26, 2010.
- [27] Y. Hattori, S. Mukasa, H. Toyota, T. Inoue, and S. Nomura, "Synthesis of zinc and zinc oxide nanoparticles from zinc electrode using plasma in liquid," *Mater. Lett.*, vol. 65, no. 2, pp. 188–190, 2011.
- [28] F. Rataboul and B. Chaudret, "Synthesis and characterization of monodisperse zinc and zinc oxide nanoparticles from the organometallic precursor $[\text{Zn}(\text{C}_6\text{H}_{11})_2]$," *J. Organomet. Chem.*, vol. 644, pp. 307–312, 2002.
- [29] G. Canizal, P. S. Schabes-Retchkiman, U. Pal, H. B. Liu, and J. A. Ascencio, "Controlled synthesis of ZnO nanoparticles by bioreduction," *Mater. Chem. Phys.*, vol. 97, no. 2–3, pp. 321–329, 2006.
- [30] Y. F. Guan and J. Pedraza, "Synthesis and alignment of Zn and ZnO nanoparticles by laser-assisted chemical vapor deposition.," *Nanotechnology*, vol. 19, no. 4, p. 045609, 2008.
- [31] B. N. Pal and D. Chakravorty, "Pattern formation of zinc nanoparticles in silica film by electrodeposition," *J. Phys. Chem. B*, vol. 110, no. 42, pp. 20917–20921, 2006.
- [32] S. R. Ghanta, M. H. Rao, and K. Muralidharan, "Single-pot synthesis of zinc nanoparticles, borane (BH₃) and closo-dodecaborate (B₁₂H₁₂)²⁻ using LiBH₄ under mild conditions.," *Dalton Trans.*, vol. 42, no. 23, pp. 8420–5, 2013.
- [33] S. Amirkhanlou, M. Ketabchi, and N. Parvin, "Nanocrystalline/nanoparticle ZnO synthesized by high energy ball milling process," *Mater. Lett.*, vol. 86, pp. 122–124, 2012.
- [34] H. M. Deng, J. Ding, Y. Shi, X. Y. Liu, and J. Wang, "Ultrafine zinc oxide powders prepared by precipitation / mechanical milling," *J. Mater. Sci.*, vol. 36, pp. 3273–3276, 2001.

- [35] A. M. Glushenkov, H. Z. Zhang, and Y. Chen, "Reactive ball milling to produce nanocrystalline ZnO," *Mater. Lett.*, vol. 62, no. 24, pp. 4047–4049, 2008.
- [36] S. Ozcan, M. M. Can, and A. Ceylan, "Single step synthesis of nanocrystalline ZnO via wet-milling," *Mater. Lett.*, vol. 64, no. 22, pp. 2447–2449, 2010.
- [37] N. Salah, S. S. Habib, Z. H. Khan, A. Memic, A. Azam, E. Alarfaj, N. Zahed, and S. Al-Hamedi, "High-energy ball milling technique for ZnO nanoparticles as antibacterial material," *Int. J. Nanomedicine*, vol. 6, pp. 863–869, 2011.
- [38] X. K. Zhu, X. Zhang, H. Wang, A. V. Sergueeva, A. K. Mukherjee, R. O. Scattergood, J. Narayan, and C. C. Koch, "Synthesis of bulk nanostructured Zn by combinations of cryomilling and powder consolidation by room temperature milling: Optimizing mechanical properties," *Scr. Mater.*, vol. 49, no. 5, pp. 429–433, 2003.
- [39] X. Zhang, H. Wang, R. O. Scattergood, J. Narayan, C. C. Koch, A. V. Sergueeva, and A. K. Mukherjee, "Studies of deformation mechanisms in ultra-fine-grained and nanostructured Zn," *Acta Mater.*, vol. 50, no. 19, pp. 4823–4830, 2002.
- [40] X. Zhang, H. Wang, R. O. Scattergood, J. Narayan, and C. C. Koch, "Mechanical properties of cryomilled nanocrystalline Zn studied by the miniaturized disk bend test," *Acta Mater.*, vol. 50, no. 13, pp. 3527–3533, 2002.
- [41] X. Zhang, H. Wang, R. O. Scattergood, J. Narayan, and C. C. Koch, "Evolution of microstructure and mechanical properties of in situ consolidated bulk ultra-fine-grained and nanocrystalline Zn prepared by ball milling," *Mater. Sci. Eng. A*, vol. 344, no. 1–2, pp. 175–181, 2003.
- [42] X. Zhang, H. Wang, J. Narayan, and C. C. Koch, "Evidence for the formation mechanism of nanoscale microstructures in cryomilled Zn powder," *Acta Mater.*, vol. 49, no. 8, pp. 1319–1326, 2001.
- [43] X. Zhang, H. Wang, M. Kassem, J. Narayan, and C. C. Koch, "Preparation of bulk ultrafine-grained and nanostructured Zn, Al and their alloys by in situ consolidation of powders during mechanical attrition," *Scr. Mater.*, vol. 46, no. 9, pp. 661–665, 2002.
- [44] U. Herr, "Mechanical Alloying and Milling," *Key Eng. Mater.*, vol. 103, pp. 113–124, 1995.
- [45] J. M. Hoey, A. Lutfurakhmanov, D. L. Schulz, and I. S. Akhatov, "A review on aerosol-based direct-write and its applications for microelectronics," *J. Nanotechnol.*, vol. 2012, 2012.

- [46] C. E. Folgar, C. Suchicital, and S. Priya, "Solution-based aerosol deposition process for synthesis of multilayer structures," *Mater. Lett.*, vol. 65, no. 9, pp. 1302–1307, 2011.
- [47] I. Grunwald, E. Groth, I. Wirth, J. Schumacher, M. Maiwald, V. Zoellmer, and M. Busse, "Surface biofunctionalization and production of miniaturized sensor structures using aerosol printing technologies.," *Biofabrication*, vol. 2, no. 1, p. 014106, 2010.
- [48] Z. Zhang, X. Zhang, Z. Xin, M. Deng, Y. Wen, and Y. Song, "Synthesis of monodisperse silver nanoparticles for ink-jet printed flexible electronics," *Nanotechnology*, vol. 22, no. 42, p. 425601, 2011.
- [49] I. Theodorakos, F. Zacharatos, R. Geremia, D. Karnakis, and I. Zergioti, "Selective laser sintering of Ag nanoparticles ink for applications in flexible electronics," *Appl. Surf. Sci.*, vol. 336, pp. 157–162, 2015.
- [50] M. Hummelgård, R. Zhang, H. E. Nilsson, and H. Olin, "Electrical sintering of silver nanoparticle ink studied by In-situ TEM probing," *PLoS One*, vol. 6, no. 2, pp. 1–6, 2011.
- [51] J. Perelaer, B. J. De Gans, and U. S. Schubert, "Ink-jet printing and microwave sintering of conductive silver tracks," *Adv. Mater.*, vol. 18, no. 16, pp. 2101–2104, 2006.
- [52] T. Kraus, L. Malaquin, H. Schmid, W. Riess, N. D. Spencer, and H. Wolf, "Nanoparticle printing with single-particle resolution," *Nat Nano*, vol. 2, no. 9, pp. 570–576, Sep. 2007.
- [53] H.-H. Lee, K.-S. Chou, and K.-C. Huang, "Inkjet printing of nanosized silver colloids," *Nanotechnology*, vol. 16, no. 10, pp. 2436–2441, 2005.
- [54] S. Jeong, K. Woo, D. Kim, S. Lim, J. S. Kim, H. Shin, Y. Xia, and J. Moon, "Controlling the thickness of the surface oxide layer on Cu nanoparticles for the fabrication of conductive structures by ink-jet printing," *Adv. Funct. Mater.*, vol. 18, no. 5, pp. 679–686, 2008.
- [55] A. Slistan-Grijalva, R. Herrera-Urbina, J. F. Rivas-Silva, M. Valos-Borja, F. F. Castilln-Barraza, and A. Posada-Amarillas, "Synthesis of silver nanoparticles in a polyvinylpyrrolidone (PVP) paste, and their optical properties in a film and in ethylene glycol," *Mater. Res. Bull.*, vol. 43, no. 1, pp. 90–96, 2008.
- [56] M. Tejamaya, I. Römer, R. C. Merrifield, and J. R. Lead, "Stability of citrate, PVP, and PEG coated silver nanoparticles in ecotoxicology media," *Environ. Sci. Technol.*, vol. 46, no. 13, pp. 7011–7017, 2012.

- [57] Q. Wei, B. Li, C. Li, J. Wang, W. Wang, and X. Yang, "PVP-capped silver nanoparticles as catalysts for polymerization of alkylsilanes to siloxane composite microspheres," *J. Mater. Chem.*, vol. 16, no. 36, p. 3606, 2006.
- [58] H. S. Shin, H. J. Yang, S. Bin Kim, and M. S. Lee, "Mechanism of growth of colloidal silver nanoparticles stabilized by polyvinyl pyrrolidone in γ -irradiated silver nitrate solution," *J. Colloid Interface Sci.*, vol. 274, no. 1, pp. 89–94, 2004.
- [59] Z. Zhang, B. Zhao, and L. Hu, "PVP Protective Mechanism of Ultrafine Silver Powder Synthesized by Chemical Reduction Processes," *J. Solid State Chem.*, vol. 121, no. 1, pp. 105–110, 1996.
- [60] B. Wiley, Y. Sun, and Y. Xia, "Synthesis of silver nanostructures with controlled shapes and properties," *Acc. Chem. Res.*, vol. 40, no. 10, pp. 1067–1076, 2007.

VITA

Bikram Kishore Mahajan was born in Agartala, India. He received his Bachelor of Technology degree in Electronics and Communication Engineering from National Institute of Technology, Agartala in 2012. He received his Masters of Technology degree in Microelectronics and VLSI Design from the same institute in 2014.

Bikram joined Missouri university of Science and Technology in May 2015 and held the positions of Graduate Research Assistant and Graduate Teaching Assistant in the department of Mechanical Engineering while working towards his Masters of Science degree at Missouri S & T. The degree of Masters of Science in Mechanical Engineering was awarded to Bikram in July 2016.